The role of inhibitory neurons in deviance sound detection in regular and random statistical contexts.

Abbreviated title: Inhibition controls deviance context dependence

Xiaomao Ding[1,2], Nathan W. Vogler[1], Melanie Tobin[1], Linda Garami[1], Alexandria M.H. Lesicko[1], Katherine C. Wood[1,3], Maria N. Geffen[1,2]

1. Department of Otorhinolaryngology, University of Pennsylvania, Philadelphia, PA, USA

2. Neuroscience Graduate Group, University of Pennsylvania, Philadelphia, PA, USA

3. University of Sheffield, Sheffield UK

*Corresponding author:
Maria Neimark Geffen, Ph.D. (she/her)
Department of Otorhinolaryngology
Perelman School of Medicine
University of Pennsylvania
5 Ravdin
3400 Spruce St.
Philadelphia PA 19104
Tel.: 215.898.0782

Number of pages: 54

Number of figures: 8 main figures + 7 supplementary figures

Conflict of Interest: The authors declare no conflicts of interest in collecting and analyzing the data and preparing this manuscript.

Acknowledgements

The authors would like to thank the members of the Geffen laboratory and Yale Cohen for discussions and helpful comments. This work was supported by the following grants from NIH: R01DC15527, R01DC014479, R03DC013660, R01NS113241 to MNG, and K99DC019504 to KCW. XD was supported by T32DC016903.

ABSTRACT

Detecting statistical regularities in sound and responding to violations of these patterns, termed deviance detection, is a core function of the auditory system. In the human brain, studies have shown that deviance responses are enhanced in regular compared to random auditory contexts, but the underlying neuronal circuit mechanisms remain unclear. Here, we examined how inhibitory neurons contribute to context-dependent deviance responses in mouse auditory cortex (AC). Using two-photon calcium imaging in AC of awake head-fixed male and female mice, we recorded neuronal activity during presentation of spectro-temporally rich moving ripple sounds, with deviant ripples embedded in either regular or random ripple sequences. AC neurons exhibited stronger responses to deviant sounds in regular contexts compared to random ones. To identify circuit mechanisms, we selectively inactivated parvalbumin (PV), somatostatin (SST), or vasoactive intestinal polypeptide (VIP) inhibitory neurons during the deviant stimulus presentation. Inactivation of PV and SST neurons broadly increased deviance responses in both contexts. In contrast, VIP inactivation selectively reduced responses to deviant stimuli in the regular, but not random, context, decreasing the context-dependent deviance signal enhancement. At the population level, inactivating all three neuronal subtypes increased detectability of the deviant stimulus, but the effects were context-dependent only for VIP inactivation. These findings reveal a distinct role for VIP neurons in modulating deviance signals based on context regularity, identifying a specific inhibitory neuron type that is critical for context-sensitive auditory processing and predictive coding.

SIGNIFICANCE STATEMENT

Understanding how the brain detects and responds to predictable and unexpected sounds is critical for communication and navigation in complex acoustic environments. Although prior studies have shown that detection of novel sounds is enhanced by regularity in background sound patterns, the underlying circuit mechanisms have remained unknown. Here, we find that neurons in the auditory cortex exhibit stronger deviance responses when the deviant sounds are embedded in regular, predictable sound sequences as compared to random sound sequences. Importantly, we identify a distinct role for specific inhibitory neurons in modulating this context-dependent enhancement. These findings reveal a new insight into how cortical circuits implement predictive coding strategies to optimize sensory processing.

INTRODUCTION

Successfully navigating everyday sound environments requires the auditory system to detect and interpret unexpected sounds within predictable patterns (Barascud et al., 2016; Sohoglu and Chait, 2016; Parras et al., 2017; Southwell and Chait, 2018). Natural sounds are characterized not only by their spectral content but also by higher-order spectro-temporal regularities: statistical relations that allow listeners to form predictions about upcoming auditory events. Detecting violations of these predictions—referred to as *deviance detection*—is a core auditory computation, supporting a wide range of behaviors, from identifying a familiar voice in a noisy crowd to detecting an approaching vehicle amid ambient noise (Arnal and Giraud, 2012). The human brain encodes both predictions and prediction errors, with signals such as the mismatch negativity (MMN) reflecting changes in neuronal activity in response to unexpected sounds (Naatanen et al., 1978, 2004, 2007). Deviance signals have been observed across multiple stages of the auditory

pathway, including the inferior colliculus (IC) (Lesicko et al., 2022), medial geniculate body (MGB) (Antunes et al., 2010; Malmierca et al., 2015), and auditory cortex (AC) (Nelken, 2004, 2014; Hershenhoren et al., 2014; Natan et al., 2015, 2017; Rubin et al., 2016; Parras et al., 2017). However, the transformations of prediction and deviance signals along this pathway, and the neural mechanisms that shape their context sensitivity, remain poorly understood.

In humans, deviance responses are enhanced when deviant sounds are embedded within regular contexts (e.g., a predictable sequence ABCD, ABCD…) as compared to random ones (e.g. shuffled sequence: BADC, ADCB…) (Sohoglu and Chait, 2016; Southwell and Chait, 2018). Stronger responses to a deviant sound following a regular pattern suggest that the brain modulates prediction strength based on context. Within AC, nearly all neurons adapt to frequently presented sounds and an enhanced response to rare, deviant stimuli (Harms et al., 2014; Parras et al., 2017) — a phenomenon known as stimulus-specific adaptation (SSA) (Ulanovsky et al., 2003; Szymanski et al., 2009; Farley et al., 2010; Natan et al., 2015). AC neurons are also sensitive to patterns with structure across multiple time scales (Ulanovsky et al., 2004; Yaron et al., 2012; Mehra et al., 2022). Here, we asked whether individual AC neurons exhibit enhanced deviance responses in regular as compared to random contexts, and whether intra-cortical inhibitory neurons support this transformation.

Inhibitory neurons in AC play distinct roles in shaping auditory cortical responses to sound patterns. The two most common subtypes, parvalbumin (PV)- and somatostatin (SST)-expressing neurons (Lee et al., 2010; Tremblay et al., 2016; Wood et al., 2017), differentially contribute to SSA and other forms of auditory adaptation (Levy and Reyes, 2012; Chen et al., 2015; Natan et al., 2015, 2017; Phillips et al., 2017), while another prominent subtype, vasoactive intestinal polypeptide (VIP)-expressing neurons, contribute to context- and state-dependent modulation (Lee

et al., 2010; Tremblay et al., 2016; Wood et al., 2017). VIP neurons gate top-down influences and can modulate predictive coding processes through a disinhibitory circuit (Pfeffer et al., 2013; Pi et al., 2013; Mesik et al., 2015; Bastos et al., 2023; Ferguson et al., 2023; Najafi et al., 2025). We hypothesized that these distinct inhibitory neuron classes differentially contribute to deviance detection depending on regular or random context.

Using two-photon calcium imaging in awake mice, we recorded neuronal activity of large populations of neurons in AC during presentation of deviant spectro-temporally complex ripple stimuli embedded in either regular or random sound contexts. We optogenetically inactivated PV, SST, or VIP neurons to determine their respective roles in modulating deviance responses. Regular context enhanced deviance responses compared to random context. This enhancement was differentially shaped by distinct inhibitory neuron classes. PV and SST inactivation increased responses to deviant sounds, but the role of context was non-specific, whereas VIP inactivation selectively reduced deviance responses in the regular, but not random context. These results identify VIP neurons as a key component of the circuit that integrates context statistics to shape deviance responses.

METHODS

Animals

A total of 14 mice (male/female) were used in this study. The strains used were: Cdh23 x PV-Cre (B6.CAST-Cdh23Ahl+/Kjn, JAX: 002756 x Pvalbtm1(cre)Arbr/J, JAX: 017320; n = 4), Cdh23xSST-Cre (B6.CAST-Cdh23Ahl+/Kjn x Ssttm2.1(cre)Zjh/J, 113 JAX: 013044; n = 4), VIP-IRES-Cre (B6.CAST-Cdh23Ahl+/Kjn x Viptm1(cre)Zjh/J, JAX: 010908; n = 3), VGAT-Cre crossed with transgenic GCaMP8m (Slc32a1tm2(cre)Lowl/J, JAX: 016962 x Igs7tm1(tetO-GCaMP8m,CAG-tTA2)Genie/J, JAX:037718, n = 3), Cdh23 (B6N(Cg)-Cdh23tm2.1Kjn/Kjn, n =

5), aged 12-26 weeks. Cdh23 mice were used because they do not exhibit age-related hearing loss which is common in C57BL/6J mice (Johnson et al., 2017). Mice were housed individually after cranial window implant and were housed on a reversed light-dark cycle. Experimental procedures were performed in accordance with NIH guidelines and approved by the IACUC at the University of Pennsylvania.

Surgery Procedures

Cranial window implants were implanted following a procedure described previously (Wood et al., 2022; Tobin et al., 2024). Mice were anesthetized with 3% isoflurane which was steadily reduced to 1.5% through the surgery. A 3 mm craniotomy was performed over the left auditory cortex with a 3 mm biopsy punch. A viral 750 nL cocktail (4:1 ratio) of virus encoding GCAMP (7f: AAV1-Syn-jGCaMP7f-WPRE, Addgene 104488 or 8m: pGP-AAV-syn-jGCaMP8m-WPRE, Addgene 162375) and virus encoding Jaws in a Cre-dependent fashion (AAV8-CAG-FLEX-JAWS-kgc-tdTomato, UNC Vector Core or AAV8-CAG-FLEX-JAWS-kgc-tdTomato, Penn Vector Core, Addgene 84446) was injected at 3 locations in the craniotomy, separated 0.3-0.5 mm apart in the anterior-posterior direction. The craniotomy was then sealed with a custom round glass window consisting of a 3 mm window glued to a 4 mm window with Norland Optical Adhesive 68. A custom-made metal headplate was attached to the skull with C&B Metabond dental cement. For transgenic GCaMP8m mice, no virus was injected and only the window implant was performed. Mice were allowed to recover for 3 weeks before imaging started.

Two-photon imaging

All imaging sessions were performed in a custom-built acoustic isolation booth using previously published methods (Betzel et al., 2019; Wood et al., 2022; Tobin et al., 2024). Mice were habituated

to being head fixed for 3 days prior to imaging. Wide-field imaging was performed on each mouse to identify sound-responsive areas of the window before two-photon imaging by presenting 3 tone pips (5kHz, 15kHz and 30 kHz) and mapping the gradients of frequency tuning and regions of reversal (Romero et al., 2020). We imaged in layer 2/3 of auditory cortex of awake head-fixed mice using a two-photon (2P) microscope (Ultima 2Pplus *in vivo* multiphoton microscope, Bruker) with a 940 nm laser (Chameleon Ti-Sapphire) with a 16X Nikon objective with a 0.8 numerical aperture (Thorlabs, N16XLWD-PF) (Figure 1 A, B, D). Recordings were made at 512 x 512 pixels and at 30 frames per second.

Optogenetic Manipulation

Optogenetic stimulation was performed using a LED (Thorlabs M625L4) delivering 625 nm light through the objective lens (Tobin et al., 2024). Before each stimulus session, the LED light power was calibrated to ~2.8 mW/mm^2 for mice injected with the virus encoding Jaws from the Penn Vector Core and ~7 mW/mm^2 for mice injected with the virus encoding Jaws from the UNC Vector Core based on reported inhibition performance of Jaws (Chuong et al., 2014). Optogenetic manipulation occurred randomly in 50% of presentations of the deviant ripple. The LED was turned on continuously for 300 ms, synced with stimulus onset, during the deviant ripple presentation. Control mice (SST-Cre, n=2) were injected with the viruses encoding tdTomato (in a Cre-dependent fashion) and GCaMP, but not Jaws (Supplementary Figure S6), and did not exhibit a significant effect of light on tuning stimulus ripple responses (N =284, linear mixed effects model, $F(1, 2978) = 3.24$, $p = 0.072$).

Acoustic stimuli

Auditory moving ripples were generated at a sampling rate of 400 kHz in MATLAB according to the following formula:

$$S(t,x) = L[1 + \Delta A sin(2\pi wt + 2\pi\Omega x + \Phi)]$$

where w (cyc/s) is the temporal modulation parameter and Ω (cyc/octave) is the spectral modulation parameter. The variable Φ represents the random phase for the envelope, ΔA represents the sinusoidal amplitude, and L represents the depth modulation. The frequency is represented as $x = log_2(\frac{f}{f_0})$, where f_0 is the lowest frequency in the stimulus (Depireux et al., 2001). Individual ripples spanned a frequency range of 5-50 kHz, lasted 300 ms, were presented at 70 dB SPL with a 15 dB modulation depth, and had a 5 ms cosine ramp applied at the beginning and end. Background sequences were generated by concatenating ripples A, B, C, and D in either a fixed sequence (REG) or a random sequence (RND) resulting in a 1.2 s stimulus (Figure 1C). The deviant sequence was generated by concatenating ripples X, Y, Z, and W in that order for all stimulus conditions. Sequences were presented with a 1 s inter-stimulus interval. Background sequences were repeated 3-6 times pseudo-randomly before a deviant sequence was presented. A control sequence of each ripple presented in isolation with a 1 s ISI was also presented to determine the base sound response of neurons.

Electrophysiology

Mice were prepared for *in vivo* electrophysiological recordings as described previously (Vogler et al., 2024). At least two weeks prior to recordings, a ground pin was inserted via small craniotomy over the left frontal cortex, and a custom-made stainless steel headplate (eMachine Shop) was secured to the skull using dental cement (C&B Metabond) and acrylic (Lang Dental) (Vogler et al., 2024). Recordings were performed in a custom-built acoustic isolation booth. At least one week following headplate surgery, mice were habituated to the recording setup for increasing durations (5-60 min) over the course of 3 days. On the day of recording, mice were anesthetized with 1.5-2.5% isoflurane, and a small craniotomy was made over the left auditory cortex using a

194 dental drill, centered ~1.5mm anterior to the lambdoid suture along the caudal end of the
195 squamosal suture. Following the craniotomy, mice were allowed to recover from anesthesia for at
196 least 30 min. Acute extracellular recordings in the auditory cortex were performed using a 32-
197 channel silicon probe (A1x32-Poly2-5mm-50s-177, NeuroNexus). The probe was positioned
198 perpendicularly to the brain surface and lowered at 1-2 μm/s to a final depth of 900-1200 μm or
199 until all channels were within the brain. During lowering of the probe, we monitored responses to
200 brief broadband noise clicks to confirm localization within auditory cortex. Neuronal signals were
201 amplified and digitized with an Intan headstage (RHD 32ch) and recorded by an OpenEphys
202 acquisition board (Siegle et al., 2017) at a rate of 30 kHz. Signals were filtered between 500 and
203 6000 Hz, offset corrected, and re-referenced to the median across all channels. Spiking data were
204 sorted using Kilosort2 (Pachitariu et al., 2016) and manually curated in phy2 to identify putative
205 single- and multi-units.

206 **Immunohistochemistry**

207 Mouse brains were extracted and sliced as previously reported (Wood et al., 2022; Vogler et al.,
208 2024). In brief, mice were anesthetized with an injection of dexmedetomidine (1 mg/kg) and
209 ketamine (120 mg/kg) and then perfused with phosphate-buffered saline (PBS) and 4%
210 paraformaldehyde (PFA). Brains were fixed in 4% PFA overnight at 4°C. Coronal slices were
211 acquired on a cryostat (Leica CM1860) at −25°C. Slices were incubated overnight at 4°C with an
212 RFP antibody (1:1000, Rockland: 600-401-379) followed by an anti-rabbit secondary for 2 hours
213 at room temperature before imaging (see representative images from VIP-Cre, PV-Cre and SST-
214 Cre mice of neurons labels with tdTomato and GCaMP in Supplementary Figure S1). Expression
215 of GCaMP was identified and cross-referenced with the Paxinos mouse brain atlas (Figure 1A
216 bottom).

Data analysis and statistics

Suite2P (Pachitariu et al., 2017) was used to register raw two-photon images, select regions of interest (ROI), and perform neuropil correction (Betzel et al., 2019; Wood et al., 2022; Tobin et al., 2024). A 0.3 Hz highpass filter was used to correct for slow fluctuations in the calcium signal. The calcium signal from each ripple sequence was converted to a z-scored $\Delta F/F_{std}$=(F-mean($F_{baseline}$))/std($F_{baseline}$) where $F_{baseline}$ is the calcium signal from the 300 ms preceding stimulus onset. An additional motion correction step was performed using PatchWarp (Hattori and Komiyama, 2022). We found that small motion artifacts during imaging induced negative transients in the calcium trace. These artifacts were identified by setting a threshold for the X and Y values from the summary stat output and any trials within 3 frames of an artifact were removed from further analysis. This removed approximately 10% of all recorded trials. For statistical comparison of responses, we computed the mean response strength during the 300 ms following the onset of a ripple on each trial. To identify neurons exhibiting significant deviance responses, we compared the responses over trials during the same ripple presented as deviant and tuning stimulus using an unpaired t-test in either random or regular context. To compare deviance response strength across neurons in different conditions, we computed mean response to the first ripple X in the deviant stimulus sequence and implemented repeated measures ANOVA with context (regular or random) and light (on or off) as two factors. We used Tukey-Kramer for post-hoc comparisons. For linear mixed effects models (LME), we used the fitlme function in MATLAB. Throughout our LME analyses, we included the recording session ID as a predictor to control for effects of session-to-session variability. If the output of the statistical test in MATLAB resulted in “p = 0”, this was most likely due to a rounding error, and we reported it as $p < 1e\text{-}20$. The results from all statistical tests are reported in Supplementary Table S1.

REGRND Index

The REGRND index was computed as the difference between the absolute values of the mean response to the deviant ripple presented in the REG and RND contexts divided by the sum of the absolute values. This provides a value between -1 and 1 where an index value close to 1 indicates that the neuron preferred to respond to the REG context, a value close to -1 indicates a preference for RND, and a value close to 0 indicates no preference.

$$REGRND_{Index} = (|REG| - |RND|)/(|REG| + |RND|)$$

Exponential Fits

Mean responses y from 0-300 ms after stimulus onset for individual trials were fit to the exponential function below:

$$y = a * e^{bx} + c$$

The variables a, b, and c were free parameters, and the variable x represented the trial presentation number. A neuron was considered to have a significant adaptation effect ($a > 0$) or facilitation effect ($a < 0$) if the RMSE from the exponential fit was less than the RMSE to the mean response. Fits were performed using MATLAB curve fitting toolbox.

SVM

Sample populations of 1, 12, 25, 50, 100, or 200 neurons were selected randomly (with replacement) from neurons within a single recording session. For each recording session, 1000 samples of responses were selected at random for each population size and average performance was reported. For each sample, the population response was represented as a vector with each entry being the mean response of a neuron 0-300 ms from stimulus onset for an individual trial. Then, a support vector machine (SVM) was trained to predict either ripple identity from the tuning stimulus or to predict the background context (REG/RND) from the responses to deviant ripple

(Vapnik, 2013; Wood et al., 2022; Tobin et al., 2024). 20% of the trials were held out as a test set while the SVM was trained on the remaining 80%.

Data and code availability

All original data and code will be made freely available upon publication. Source data will be deposited in a Dryad data depository. Data analysis code will be available on GitHub: https://github.com/geffenlab/Ding_2025.

RESULTS

Characterizing the sound response to individual moving ripples

We imaged calcium activity in populations of neurons in layer 2/3 of auditory cortex (AC) in awake, head-fixed mice presented with a series of sequences of spectro-temporally complex sounds (termed "moving ripples") (Figure 1 A-D). Each ripple was comprised of a broadband sound with the envelope and frequency modulation varying in time. For the regular (REG) and random (RND) background ripples, we used the same 4 ripples (300 ms long, 5-50 kHz, 70 dB SPL mean intensity), which were repeated in the same sequence (REG; ABCD, ABCD, ABCD, …), or in varying order (RND; BADC, BDAC, CBDA, …). Each background sequence consisted of 3-6 repeats of the 4 ripples with 1 s inter-repeat interval followed by the deviant ripple sequence. Because the background sequence is comprised of the same ripples in both REG and RND, the only difference between the two contexts is the temporal order. The deviant sequence of ripples included 4 different ripples from those used in the background. These ripples were in the same frequency range but had different modulation frequencies. Additionally, the ripples were also presented individually with a 1 sec interstimulus interval to construct baseline tuning responses.

This stimulus allowed us to test multiple aspects of the neuronal responses to sounds in varying statistical regimes. First, we tested whether a given ripple evoked a greater or smaller neuronal response when it was unexpected. Second, we tested whether a deviant ripple elicited a greater or smaller response in the regular or random context. Third, we tested whether the responses to the context ripples differed when they were presented in regular or random context, and whether adaptation to their presentation over subsequent repeats differed based on whether their order was regular or random. We expected the responses to deviant ripples to be greater than the respective baseline sound response. We also expected deviance responses to be greater in the regular than random context. Finally, we expected adaptation to repeated ripple sequences to be stronger for regular than random contexts.

We recorded activity from 8,573 neurons in the AC, with 76.6% (n = 6,566) showing a significant sound response to at least one ripple (z-scored averaged fluorescent response 0-300 ms post stimulus-onset versus the average fluorescence 0-300 ms before stimulus on each trial, t-test with a Bonferroni correction for the number of ripples). The fluorescence of neurons typically increased over the first 200 ms after sound presentation followed by a gradual decrease in fluorescence (representative neurons, Figure 1E, F). Across all imaged neurons, 22.4% (n = 1,922/8,573) responded to only one ripple while 6.3% (n = 541/8,573) had significant responses to all eight ripples. Additionally, the fraction of responsive neurons to each ripple was relatively even across all eight ripples, with a maximum difference of 22.4% (Figure 1G, H, Supplementary Figure S3). Whereas many neurons exhibited an enhancement in fluorescence in response to the ripples (n = 1,967/6,566), the majority of imaged neurons exhibited a suppression in fluorescence to individual ripples (n = 4,599/6,566, Figure 1I). The suppression in fluorescence corresponds to a decrease in calcium concentration, which most likely is due to reduced spiking activity in

response to the moving ripples (Attinger et al., 2017; Solyga and Keller, 2025). We then split the distribution of responses by mouse line (VIP-cre, PV-cre, and SST-cre) and found similar results. The majority of neurons from each line responded only to 1 ripple (VIP: 27.2%, PV: 31.3%, SST: 33.3%) and responses to ripples were relatively even across all eight ripples (maximum difference, VIP: 19.4%, PV: 26.1%, SST: 31.6%) with negative responses forming the majority (Supplementary Figure S3 A, B, C right). Furthermore, mean response strengths to tuning stimuli were similar across all three mouse lines (approximately -0.2 z-scored delta F/F, Supplementary Figure 7 A, B, C solid lines). When appropriate, we analyzed the positive responses as a separate group from negative responses. Combined, responses to individual ripples demonstrate that these stimuli efficiently drive neuronal calcium responses in AC.

Regularity of context modulates deviance response

Most neurons in AC that we imaged exhibited a deviance response: 51.2% of neurons exhibited a stronger response to the deviant ripple in either the RND or REG condition as compared to the tuning response (significant change in mean response within the 300 ms window post-stimulus onset to the deviant ripple compared to tuning response to that ripple, N = 4,391 responsive neurons out of 8,573 neurons recorded). There was a significant effect of deviance on the response to the same ripple (n = 4,391, repeated measures ANOVA, $f(2) = 51.18$, $p = 7.95e-23$). These deviance responses were significant when computed separately for the positive (n = 2,429, repeated measures ANOVA, $f(2) = 1816.91$, $p < 1e-20$, Figure 2A-D) and negative (n = 1,962, repeated measures ANOVA, $f(2) = 1324$, $p < 1e-20$, Figure 2F, G, H) responding neurons. The remaining neurons (n = 4,182) exhibited no significant difference in response to the deviant ripple compared to its baseline response (Figure 2J, K, L). Deviance responses were also

significant for a group that included neurons with both positive deviance and baseline responses (n = 191, repeated measures ANOVA, f(2) = 129.72, p = 1.14e-43, Figure 2N, O, P).

For neurons with positive deviance responses, the REG context enhanced the deviance response in the corresponding direction. The deviance response magnitude was greater under the REG context than under the RND context (lme: F(1, 7284) = 121.761, p< 1e-20, Figure 2B, C, D). The context-dependent difference in deviance response strength persisted when we considered neurons with both positive deviance and baseline sound responses to the deviant ripple (lme: F(1, 570) = 65.161, 4.11E-15, Figure 2N, O, P). For negative-responding neurons, the difference in deviance response between the REG and RND contexts was not significantly different (lme: F(1, 5883) = 0.719, p = 0.4, Figure 2G, H). Similarly, neurons that did not exhibit significant deviance responses did not have a preference for the REG context (lme: F(1, 12543) = 2.965, p = .085, Figure 2J, K, L). For positive deviance responses, these results are consistent with our predictions, as we expected the deviance response to be stronger in the regular compared to random conditions. We note that a substantial fraction of neurons exhibited negative calcium responses to sound stimulation, with a distribution of responses similar across the VIP-Cre, PV-Cre and SST-Cre lines (Supplementary Figure S2). Similar suppressive signals in auditory cortex have been documented by other groups (e.g., Solyga and Keller, 2025; Tsukano et al., 2025), suggesting this is a reproducible phenomenon, but it is difficult to interpret negative novelty responses as a larger negative response may be a combination of a stronger or weaker interactions. Importantly, our key effects—including context-dependent deviance responses—were robust across different subsamples (Figure 2).

To further account for possible differences in responses by mouse line as well as any potential bias from our selection criteria, we separately analyzed our data from VIP-cre, PV-cre,

354 and SST-cre mice (Supplementary Figure S4). We first selected neurons that showed a significant
355 difference between REG and RND deviance responses and then split into populations with a
356 positive or negative deviance response. For positive deviance response, we found that REG
357 responses were significantly greater than RND responses across all three mouse lines (LME, VIP-
358 Cre: N = 648, p< 1e-20, PV-Cre: 350, p=6.12e-5, SST-Cre: N = 107, p=.0009; Supplementary
359 Figure S4 A, C, E). For only negative responses, we did not observe consistent differences across
360 the three mouse lines, and context had varying effect on negative deviance (LME, VIP-Cre: N =
361 519, p = .32, PV-Cre: N = 274, p = .16; SST-Cre: N = 102, p = .0009; Supplementary Figure S4B,
362 D, F). The effect in positive novelty responses is consistent with our hypothesis and results across
363 all mouse lines.

364 To further understand the preference of individual neurons' deviance responses for
365 temporal context, we computed a REGRND index (see Methods) which ranged from -1 to 1, with
366 -1 indicating a preference for the RND context and 1 indicating a preference for the REG context.
367 For positive deviance responses, we found that a majority of neurons only exhibited a significant
368 deviance response in one of the REG (43.8%) or the RND (24.5%) contexts. For neurons exhibiting
369 a significant deviance response in both contexts, we found a significant preference for the REG
370 context when considering the REGRND index (mean = 0.06, t-test, p = 1.31e-10, Figure 2E). This
371 preference for the REG context was stronger when we only considered neurons with a positive
372 deviance response and a positive baseline sound response (mean = 0.12, t-test, p =0.0046, Figure
373 2Q). On the other hand, neurons with negative deviance responses exhibited a small difference in
374 the percentage of neurons selective for the REG (36.9%) and RND (30.8%) contexts and no
375 significant difference in the REGRND index for neurons responsive in both (mean = 0.015, t-test,
376 p = 0.14, Figure 2I). Thus, positive deviance responses increase in magnitude as well as in the

fraction of responsive neurons in the REG over RND contexts, whereas negative deviance responses have mixed context-dependent effects.

We next analyzed how the deviance response changes over the course of an entire REG or RND stimulus block. Previous work has shown that adaptation in AC occurs over multiple time scales (Ulanovsky et al., 2004). We hypothesized that temporal regularity may also impact adaptation on longer time scales in a similar manner, with stronger adaptation occurring in the REG context compared to the RND context. We fit an exponential response function to the time course of per trial responses from individual neurons (Figure 3A, B, E). We found that a sizeable fraction of neurons exhibited long term adaptation (48.03%) or facilitation (41.52%) to the deviant ripple presentation. Neurons adapted or facilitated faster in the REG as compared to RND context (Figure 3C, D, F, G): time constants for both adaptation and facilitation were greater in the RND context than the REG context ($n_{adapt\ REG}$ = 2,545, $n_{facil\ REG}$ = 2,032, $n_{adapt\ RND}$ = 2,224, $n_{facil\ RND}$ = 1,843, 2-way ANOVA, $f(1) = 10.29$, $p = 0.0044$), indicating that context has a secondary effect on the long-term adaptation of neuronal responses to the deviant ripple. These results demonstrate a secondary mechanism for adaptation to stimulus context during deviance detection.

Cortical neurons exhibit differential spiking responses to deviant ripples in regular and random contexts

To resolve finer temporal information in cortical responses, we next performed electrophysiological recordings in the auditory cortex of awake mice (n = 5) while presenting the ripple stimuli (Figure 4A-C). From these recordings, we identified deviance responsive units using a paired t-test between the spike rates from the 300 ms following stimulus onset when the ripple was presented in isolation versus as a deviant and found that most neurons exhibited a deviance

response in either context (55%, n = 164 neurons). Among the units with a significant deviance response, 59% responded with an increase in firing rate (n = 96 neurons). When comparing the firing rates in response to the deviant ripple in the REG and RND contexts, there was a significant effect of context in the first 100 ms of the response (Figure 4D, E, repeated measures ANOVA, $f(2) = 9.36$, $p = 0.00011$). Deviance responses in the REG context were significantly greater than those in the RND context (post-hoc Tukey-Kramer, $p = 0.024$). Furthermore, the differential effect of context extended to the first 100 ms of the second (paired t-test, $p = 0.017$) and third (paired t-test, $p = 0.019$) ripples in the deviant sequence but not the fourth (paired t-test, $p = 0.093$). When examining the last 100 ms of the response to the first ripple, although the mean firing rate was higher in the REG context (~10.2 Hz) compared to the RND context (~9.2 Hz), there was no significant effect of context (repeated measures ANOVA, $f(2) = 2.022$, $p = 0.13$). These results indicate that the information about context is integrated early in the responses of neurons in AC and support our findings from 2-photon imaging.

Cortical inhibitory neurons exhibit contextually modulated deviance responses

Inhibitory neurons modulate deviance responses in AC (Natan et al., 2015; Yarden et al., 2022) as well as other sensory areas (Millman et al., 2020; Furutachi et al., 2024). In AC, cortical inhibitory neurons also exhibit the enhanced deviance response associated with SSA (Natan et al., 2015). We investigated whether cortical inhibitory neurons exhibit a similar deviance response to our ripple stimulus by imaging from a VGAT-Cre mouse line crossed with a transgenic Cre-dependent GCaMP8m line. This crossed line results in GCaMP8m expression only in inhibitory neurons. We found that, similar to our results from our pan-neuronal recordings, inhibitory neurons also exhibit a context-modulated deviance response (Figure 5). We found that 74.3% of cortical inhibitory neurons exhibited a significant deviance response. The REG context enhanced the

424 response compared to the RND context for positive responses (lme: $F(1, 2592) = 152.299$, $p < 1e-$
425 20, Figure 5C-E), and negative responses in the REG context were slightly stronger than in the
426 RND (lme: $F(1, 3426) = 3.99$, $p = .046$, Figure 5G-I). In a subset of recording sessions, we
427 presented a control stimulus sequence where the ripples used (ABCD or XYZW) for the
428 background and deviant sequences were swapped. Neurons from these sessions also exhibited an
429 enhanced deviance response in the REG context compared to the RND context (lme: $F(1, 771) =$
430 112.939, $p < 1$ e-20, Figure 5O-Q). The REGRND index from the inhibitory neurons followed a
431 similar pattern to our results from the general neuronal recordings. For positive responses, there is
432 a significant preference for the REG context in neurons responsive to both contexts in the original
433 (REGRND index mean = 0.098, t-test, $p = 1.31e-10$, Figure 5F) and control sequences (REGRND
434 index mean = 0.154, t-test, $p =7.02e-9$, Figure 5R), while no significant effect was observed for
435 negative responses (REGRND index mean = 0.012, t-test, $p = 0.25$, Figure 5J). Furthermore, the
436 inhibitory neuronal population that did not exhibit a significant deviance response had a slightly
437 stronger novelty sound response in regular condition, although this relation was not significant in
438 a post-hoc test (lme: $F(1, 2085) = 6.537$, $p = 0.011$, post-hoc Tukey-Kramer, n.s., Figure 5K-N).
439 The large fraction of context-sensitive inhibitory neurons and strong context-evoked differences
440 in the deviance responses in inhibitory neurons indicate that the deviance response found in the
441 general population may be controlled by inhibitory neurons.
442

443 **Optogenetic inactivation of inhibitory neurons differentially modulates deviance responses**

444 We next asked how specific classes of inhibitory neurons modulate cortical deviance
445 detection in different contexts. Previous work has shown that PV and SST neurons differentially
446 modulate stimulus-specific and temporal adaptation in AC (Natan et al., 2015, 2017). VIP neurons

form a disinhibitory circuit with SST neurons and have also been shown to modulate deviance responses in sensory cortex (Furutachi et al., 2024). Therefore, we hypothesized that these distinct inhibitory neuron classes differentially modulate deviance responses in regular and random contexts. To investigate the role of inhibitory neurons in modulating the deviance response, we measured calcium activity in AC neurons while inactivating PV, SST, or VIP neurons using optogenetic activation of Jaws on a subset of trials (Figure 6A-D). Jaws is a red-shifted inhibitory opsin which we expressed selectively in each of three interneuron subtypes using Cre-expressing transgenic mice. We inactivated each of the three inhibitory neuron classes during the presentation of the first ripple in the deviant sequence to identify their selective role in modulating the response. As expected, inactivating VIP neurons decreased response amplitude to ripples, whereas inactivating SST or PV neurons increased the responses to ripples (Figure 6E-P, Figure S5, solid and dashed lines).

For neurons with a positive deviance response, inactivation of VIP neurons decreased the amplitude of the tuning response to the ripples (paired t-test, $p < 1e\text{-}20$, Figure 6E, F). The effect of VIP neurons on deviance responses was selective for the temporal context (linear mixed effects model, $F(1,5416) = 43.57$, $p= 4.48e\text{-}11$, Figure 6E-H): suppressing VIP neurons significantly reduced the deviance response in the regular ($F(1,5416) = 80.01$, $p < 5.02e\text{-}19$), but not random contexts ($F(1,5416) = 0.15$, $p = 0.70$, Figure 6F, G). Inactivating PV or SST neurons increased tuning responses to the ripple, changing the mean response from negative to positive (paired t-test, $p_{PV} < 1e\text{-}20$, $p_{SST} < 4.19e\text{-}29$, Figure 6I, J, M, N). Inactivating PV or SST neurons increased the deviance response for both REG ($F_{PV}(1, 3364) = 44.57$, $p_{PV} =2.86e\text{-}11$, Figure 6I-L, F_{SST} $(1, 924) = 24.07$, $p_{SST} = 1.1e\text{-}6$, Figure 6M-P) and RND ($F_{PV}(1, 3364) = 53.76$, $p_{PV} =2.82e\text{-}13$, Figure 6I-L, F_{SST} $(1, 924) = 31.18$, $p_{SST}= 3.1e\text{-}8$, Figure 6M-P) contexts. However, there was no difference

470 in the increase in deviance response due to the temporal context (linear mixed effects model, F_{PV}
471 (1,3364) = 0.22, p_{PV} (Context x Light) = 0. 64, Figure 6K, L, F_{SST}(1,924) = 0.32, p_{SST} (Context x
472 Light) = 0.63, Figure 6O, P). We also fit a linear mixed effects model to test whether the observed
473 difference in context dependent light modulation was significantly across mouse lines. Inactivation
474 of VIPs was the only significant context dependent effect in this model (linear mixed effects model,
475 F_{VIP}(1,2426) = 31.95, p_{VIP} = 1.76e-8; F_{PV}(1,2426) = 0.339, p_{PV} = 0.56; F_{SST}(1,2426) = 0. 653, p_{SST}
476 = 0. 42). Furthermore, the difference in effect between VIP and PV (linear mixed effects model,
477 F(1,2426) = 7.13, p = 0.0077) and VIP and SST (linear mixed effects model, F(1,2426) = 7.95, p
478 = 0.0049) was significant while the difference between PV and SST was not (linear mixed effects
479 model, F(1,2426) = 0.083, p = 0. 77). Thus, VIP neurons selectively control the deviance responses
480 in REG, but not RND context, whereas PV and SST neurons reduce deviance responses in a
481 context-independent fashion.

482 For neurons that have negative deviance responses, optogenetic inactivation of all three
483 interneuron classes modulated the activity during the deviant stimulus (Supplementary Figure S7).
484 For negative deviance responses, inactivating VIP neurons decreased the amplitude of deviance
485 responses under both random and regular contexts (linear mixed effects model, F(1,4244) =
486 196.62, p = 1.06e-43, Supplementary Figure S7E-H). This modulation of deviance responses was
487 not significantly context-dependent (linear mixed effects model, F(1,4244) = 2.78, p(Context x
488 Light) = 0. 095, Supplementary Figure S7G, H). Inactivating PV and SST neurons increased the
489 deviance responses under both regular and random contexts (linear mixed effects model,
490 F_{PV}(1,2644) = 217.523, p_{PV} = 2.27e-47; F_{SST}(1,948) = 74.88, p_{SST} = 2.12e-17, Supplementary
491 Figure S7I-P). This change in deviance response was not context-dependent for either PV or SST
492 neuron inactivation (PVs: F_{PV}(1,2644) = 0.078, p = 0.78; SSTs: F_{SST}(1,948) = 0.67, p = 0.41,

Supplementary Figure S7K, L, O, P).These results suggests that the differential function of VIPs may be limited to positive novelty responses.

To understand how, across the positive and negative deviance responses, the inhibitory neurons affected deviance detection, we trained a support vector machine (SVM) classifier to differentiate between responses to a deviant ripple and a context ripple (Figure 7A). For each recording session, we trained the classifier on the responses to the deviant ripple X versus responses to the first ripple in the repeated background sequence. To match the position in the sequence as much as possible, we used the last repeat prior to the deviant ripple on each trial. For regular contexts, this was always A, whereas for random contexts, this ripple varied between A, B, C and D. We compared the performance of the classifier in predicting whether neuronal responses corresponded to the deviant or context ripple for trials with light (when the inhibitory neurons were suppressed) and without light, for the three different inhibitory neuron types.

We found that inactivating VIP neurons differentially modulated the classifier performance, reducing it only for the regular context condition, but not for the random context (post-hoc Tukey-Kramer, $p_{REG} < 0.00036$, post-hoc Tukey-Kramer, $p_{RND} < 0.85$, Figure 7B, C). In contrast, inactivating PV or SST neurons improved SVM performance under both random (post-hoc Tukey-Kramer, $p_{PV} < 0.00017$, post-hoc Tukey-Kramer, $p_{SST} < 4.98e-9$, Figure 7E, G) and regular (post-hoc Tukey-Kramer, $p_{PV} < 7.76e-7$, post-hoc Tukey-Kramer, $p_{SST} < 1.28e-7$, Figure 7D, F) contexts. These results are in line with the changes in the mean response strength that we observed (Figure 6). They furthermore suggest that the selective effects of inactivating VIP neurons for REG context persist for the discriminability of deviant stimuli, whereas PV and SST neurons affect deviance responses, but not in a context-independent fashion.

We next asked more broadly how these changes in deviance detection are implemented across the population of AC neurons. We expanded the discriminability analysis to multiple discrimination schemes and used subsets of progressively increasing numbers of neurons to train the SVMs. We found that discriminability increased with the number of neurons in the analysis and did not saturate at 200 neurons for any discrimination scheme (Figure 8A, B).

First, to establish a baseline in ripple discriminability based on the tuning stimulus, we computed the effect of inactivation of inhibitory neurons on discriminability between two ripples (Figure 8A left). PV and SST inactivation led to an increase in ripple discriminability, reaching higher than 90% discriminability at n = 200 neuron population size (2-way ANOVA, f(1) = 27.50, p_{PV} = 5.094e-6, Figure 8D; 2-way ANOVA, f(1) = 58.62, p_{SST} = 1.98e-9, Figure 8E). VIP inactivation had a significant, but much weaker effect (2-way ANOVA, f(1) = 7.45, p = 0.0072, Figure 8C, D, E). These results are consistent with prior studies that found that PV and SST neurons affect neuronal tuning properties (Aizenberg et al., 2015; Li et al., 2015; Natan et al., 2015, 2017; Phillips and Hasenstaub, 2016; Kato et al., 2017; Phillips et al., 2017), whereas VIP neurons have an inconsistent effect on tuning in AC (Mesik et al., 2015; Tobin et al., 2024).

Next, we compared the SVM performance in discriminating the deviance response under REG versus RND contexts. If VIP neurons play a selective role in providing context-dependent information, we expected that their inactivation would impair the discriminability of deviance responses across REG and RND contexts. By contrast, for PV and SST neurons, we expected that their inactivation would have little effect on context discriminability. Indeed, we found that inactivating VIP neurons impaired context discriminability of deviance responses, which is consistent with a decrease in the difference in deviance responses under the two contexts (2-way ANOVA, f(1) = 10.058, p = 0.0019, Figure 8F). PV inactivation did not have a significant effect

on context discriminability (Figure 8G), whereas SST inactivation improved the discriminability performance (2-way ANOVA, f(1) = 12.47, p = 0.001, Figure 8H).

Finally, we asked whether deviance detection under the two contexts improved with inhibitory neuronal inactivation. Surprisingly, we found that at a population level, inactivating all inhibitory neuron classes -- VIP, PV and SST neurons -- improved deviance detectability in REG context (2-way ANOVA, f(1) = 20.54, p_{VIP} =1.26e-5, 2-way ANOVA, f(1) = 50.18, p_{PV} = 1.26e-8, 2-way ANOVA, f(1)=58.45, p_{SST} =2.05e-9, Figure 8I, J, K). In RND context, VIP inactivation did not have an effect, whereas PV or SST inactivation also drove an improvement in deviance detection (2-way ANOVA, f(1) = 29.35, p_{PV} = 2.90e-6, 2-way ANOVA, f(1) = 75.31, p_{SST} = 7.92e-11, Figure 8 L, M, N). The effect PV or SST inactivation was strongest around a population of n = 10-25 neurons (Figure 8P, Q), suggesting that just a relatively small number of neurons can be involved in deviance detection. By contrast, the effect of VIP inactivation on deviance detection in REG context increased with increasing number of neurons (Figure 8O), suggesting that VIP neurons transmit the information about context to larger cortical populations. The finding that deviance detection at population level is increased when any of the three inhibitory neuron types are inactivated suggest that the cortical circuits operate in suboptimal regime in everyday hearing, potentially allowing for context-dependent modulation by different inhibitory neuronal classes (Tobin et al., 2024). This modulation is specific to regular context only for VIP neurons, in line in our analysis of their differential effect on single neuronal responses (Figure 6).

DISCUSSION

In this study, we investigated how statistical regularity in sound sequences influences cortical responses to deviant auditory stimuli, and how inhibitory neurons contribute to this

561 process. Using calcium imaging and optogenetic inactivation in awake mice, we found that
562 auditory cortex (AC) neurons exhibited stronger deviance responses when deviant sounds followed
563 a regular context compared to a random one. This enhancement was not uniform across cell types:
564 while PV and SST interneuron inactivation broadly increased deviance responses with mixed
565 effect of context, inactivation of VIP neurons selectively reduced deviance responses in the regular
566 context. These findings reveal a distinct role for VIP neurons in modulating context-dependent
567 deviance detection in AC.

568 Our results align with human studies showing that deviance detection is enhanced by
569 temporal predictability in sound streams. Previous EEG and behavioral work demonstrated that
570 listeners respond more robustly to violations in regular versus random sequences, but the
571 underlying neural circuitry was unknown (Barascud et al., 2016; Sohoglu and Chait, 2016;
572 Southwell and Chait, 2018). The stimuli used in these studies were comprised of pure tones
573 presented in sequences with varied temporal statistics, either random or regular. While our stimuli
574 use complex sounds (moving ripples) as the building blocks, the main stimulus manipulation we
575 investigated is still changes to the temporal context. By probing neuronal subtypes in mouse AC,
576 we provide direct evidence for circuit-level modulation of deviant responses by context. Our
577 results suggest that temporal regularity enhances deviance detection not merely by boosting
578 adaptation or prediction error in individual neurons (Ulanovsky et al., 2003, 2004; Natan et al.,
579 2015, 2017; Parras et al., 2017), but through targeted engagement of specific inhibitory networks.

580 A key contribution of this work is identifying VIP neurons as selective modulators of
581 context-dependent deviance responses. While VIP neurons have been implicated in disinhibitory
582 circuits across sensory cortical regions (Mesik et al., 2015; Pakan et al., 2016; Kuchibhotla et al.,

583 2017; Cone et al., 2019; Millman et al., 2020; Myers-Joseph et al., 2024; Tobin et al., 2024) and
584 have been implicated in oddball and unexpected stimulus responses (Yarden et al., 2022; Bastos et
585 al., 2023; Ferguson et al., 2023; Najafi et al., 2025), their role in encoding statistical structure in
586 naturalistic auditory stimuli was previously untested. We show that VIP inactivation abolished the
587 enhancement of deviance responses in the regular context without affecting responses in the
588 random context. This selective effect suggests that VIP neurons integrate contextual information—
589 potentially from top-down projections (Askew et al., 2019; Apicella and Marchionni, 2022;
590 Ferguson et al., 2023) — to gate prediction error signaling (Friston and Kiebel, 2009; Friston,
591 2010; Heilbron and Chait, 2018). In contrast, PV and SST neurons modulate gain and adaptation
592 more uniformly, regardless of context, consistent with their established roles in first-order sensory
593 processing.

594 Our findings also have implications for how auditory scenes are represented at the
595 population level. Using SVM-based decoding, we found that context information was more easily
596 extracted from single-neuron responses in the regular condition, while population-level decoding
597 performance plateaued more quickly. This shift toward a distributed, redundant code in regular
598 contexts may reflect a network reorganization mediated by VIP neurons, as previously shown in
599 auditory cortex (Tobin et al., 2024). Interestingly, inactivation of all interneuron types improved
600 decoding of deviant stimulus identity, suggesting that inhibition refines but also constrains the
601 dynamic range of population responses.

602 One strength of our approach is the use of spectrally rich ripple stimuli, which elicit reliable
603 responses in a broad population of AC neurons. These stimuli better approximate the complexity
604 of natural sounds than pure tones and may engage higher-order auditory computations relevant to

speech, communication, and environmental navigation. Our observation that deviance detection operates robustly across both excitatory and inhibitory populations reinforces the idea that prediction-related computations are a core function of auditory cortex.

This work also opens new questions about the origins of context signals that modulate VIP activity. VIP neurons are known to receive input from neuro-modulatory and associative cortical areas, including prefrontal cortex (Kuchibhotla et al., 2017; Askew et al., 2019; Apicella and Marchionni, 2022; Ferguson et al., 2023; Ramamurthy et al., 2023). The selectivity of VIP modulation for regular contexts may arise from top-down prediction signals that are absent in random sequences. Future studies using pathway-specific manipulations or recordings in interconnected regions will be needed to determine how these inputs shape VIP function (Furutachi et al., 2024).

Several caveats warrant consideration. First, while we focused on layer 2/3 pyramidal neurons, different interneuron subtypes span cortical layers and exhibit layer-specific functions. Our widefield optogenetic inactivation likely affected VIP, PV, and SST neurons in multiple layers, and the net effect observed in superficial recordings may reflect combined contributions from distinct circuits (Meyer et al., 2011; Tremblay et al., 2016; Yavorska and Wehr, 2016; Naka et al., 2019; Wu et al., 2022; David et al., 2023). Second, the precise nature of the statistical computations—adaptation versus prediction error—encoded by each subtype remains to be disentangled. Simultaneous recordings across AC layers and subcortical regions could further clarify how prediction errors are computed and propagated.

In our recordings, we observed a substantial fraction of neurons with negative calcium responses to repeated sounds (Figures 2, 5). Although less frequently emphasized in the literature,

627 such suppressive calcium signals in auditory cortex have been reported by multiple groups(Kato
628 et al., 2015; Solyga and Keller, 2025; Tsukano et al., 2025). Notably, ACx neurons exhibited net
629 negative calcium responses to auditory stimuli while showing positive responses to visual inputs,
630 suggesting a modality-specific phenomenon rather than a technical artifact(Solyga and Keller,
631 2025). The mechanisms underlying these negative signals remain incompletely understood. One
632 possibility is that calcium imaging captures inhibitory neurons more comprehensively than
633 extracellular electrophysiology, which is biased toward larger excitatory neurons, though our prior
634 labeling experiments indicate inhibitory cells are only a minority of the imaged population (Tobin
635 et al., 2024). Furthermore, with habituation to sounds over days (which we perform in our
636 experiments), the relative fraction of suppressive responses increases (Kato et al., 2015).
637 Facilitating this may be a non-linear transfer function between spiking and GCaMP fluorescence,
638 such that decreases in activity produce larger or more detectable fluorescence changes than modest
639 increases in spiking. Regardless of their precise origin, our main conclusions are robust to response
640 polarity: when analyses are restricted to neurons with positive responses, the key effects—
641 particularly the context-dependent deviance responses—remain unchanged. These observations
642 underscore the importance of reporting the full range of neuronal responses and highlight the need
643 for future work combining intracellular recordings with calcium imaging to resolve the spiking-
644 to-fluorescence relationship in suppressive responses.

645 In summary, our study demonstrates that statistical context modulates deviance detection
646 in auditory cortex through specific inhibitory circuits. We identify inhibitory neurons, and
647 specifically VIP neurons, as key players in shaping deviant responses based on contextual
648 statistical structure. These findings support models of predictive coding in sensory cortex and
649 suggest that context-sensitive disinhibition is a fundamental mechanism for flexible sensory

processing. By revealing how different inhibitory neurons contribute to deviance detection under structured versus random auditory regimes, our results advance understanding of the neuronal basis of auditory perception in complex environments.

Bibliography

Aizenberg M, Mwilambwe-Tshilobo L, Briguglio JJ, Natan RG, Geffen MN (2015) Bidirectional Regulation of Innate and Learned Behaviors That Rely on Frequency Discrimination by Cortical Inhibitory Neurons. PLoS Biology 13.

Antunes FM, Nelken I, Covey E, Malmierca MS (2010) Stimulus-specific adaptation in the auditory thalamus of the anesthetized rat. PloS one 5:e14071.

Apicella A junior, Marchionni I (2022) VIP-Expressing GABAergic Neurons: Disinhibitory vs. Inhibitory Motif and Its Role in Communication Across Neocortical Areas. Front Cell Neurosci 16 Available at: https://www.frontiersin.org/articles/10.3389/fncel.2022.811484 [Accessed April 26, 2024].

Arnal LH, Giraud A-L (2012) Cortical oscillations and sensory predictions. Trends in Cognitive Sciences 16:390–398.

Askew CE, Lopez AJ, Wood MA, Metherate R (2019) Nicotine excites VIP interneurons to disinhibit pyramidal neurons in auditory cortex. Synapse 73:e22116.

Attinger A, Wang B, Keller GB (2017) Visuomotor Coupling Shapes the Functional Development of Mouse Visual Cortex. Cell 169:1291-1302.e14.

Barascud N, Pearce MT, Griffiths TD, Friston KJ, Chait M (2016) Brain responses in humans reveal ideal observer-like sensitivity to complex acoustic patterns. Proceedings of the National Academy of Sciences 113:E616–E625.

Bastos G, Holmes JT, Ross JM, Rader AM, Gallimore CG, Wargo JA, Peterka DS, Hamm JP (2023) Top-down input modulates visual context processing through an interneuron-specific circuit. Cell Reports 42:113133.

Betzel RF, Wood KC, Angeloni C, Geffen MN, Bassett DS (2019) Stability of spontaneous, correlated activity in mouse auditory cortex. PLOS Computational Biology 15:e1007360.

Chen I-W, Helmchen F, Lütcke H (2015) Specific Early and Late Oddball-Evoked Responses in Excitatory and Inhibitory Neurons of Mouse Auditory Cortex. J Neurosci 35:12560–12573.

Chuong AS et al. (2014) Noninvasive optical inhibition with a red-shifted microbial rhodopsin. Nature neuroscience 17:1123.

Cone JJ, Scantlen MD, Histed MH, Maunsell JHR (2019) Different Inhibitory Interneuron Cell Classes Make Distinct Contributions to Visual Contrast Perception. eNeuro 6:ENEURO.0337-18.2019.

David F, Borel M, Ayub S, Ruther P, Gentet LJ (2023) Layer-specific stimulations of parvalbumin-positive cortical interneurons in mice entrain brain rhythms to different frequencies. Cereb Cortex 33:8286–8299.

Depireux DA, Simon JZ, Klein DJ, Shamma SA (2001) Spectro-Temporal Response Field Characterization With Dynamic Ripples in Ferret Primary Auditory Cortex. Journal of Neurophysiology 85:1220–1234.

Farley BJ, Quirk MC, Doherty JJ, Christian EP (2010) Stimulus-Specific Adaptation in Auditory Cortex Is an NMDA-Independent Process Distinct from the Sensory Novelty Encoded by the Mismatch Negativity. J Neurosci 30:16475–16484.

Ferguson KA, Salameh J, Alba C, Selwyn H, Barnes C, Lohani S, Cardin JA (2023) VIP interneurons regulate cortical size tuning and visual perception. Cell Rep 42:113088.

Friston K (2010) The free-energy principle: a unified brain theory? Nat Rev Neurosci 11:127–138.

Friston K, Kiebel S (2009) Predictive coding under the free-energy principle. Philosophical Transactions of the Royal Society B: Biological Sciences 364:1211–1221.

Furutachi S, Franklin AD, Aldea AM, Mrsic-Flogel TD, Hofer SB (2024) Cooperative thalamocortical circuit mechanism for sensory prediction errors. Nature 633:398–406.

Harms L, Fulham WR, Todd J, Budd TW, Hunter M, Meehan C, Penttonen M, Schall U, Zavitsanou K, Hodgson DM, Michie PT (2014) Mismatch Negativity (MMN) in Freely-Moving Rats with Several Experimental Controls. PLOS ONE 9:e110892.

Hattori R, Komiyama T (2022) PatchWarp: Corrections of non-uniform image distortions in two-photon calcium imaging data by patchwork affine transformations. Cell Reports Methods 2:100205.

Heilbron M, Chait M (2018) Great Expectations: Is there Evidence for Predictive Coding in Auditory Cortex? Neuroscience 389:54–73.

Hershenhoren I, Taaseh N, Antunes FM, Nelken I (2014) Intracellular correlates of stimulus-specific adaptation. The Journal of neuroscience : the official journal of the Society for Neuroscience 34:3303–3319.

Johnson KR, Tian C, Gagnon LH, Jiang H, Ding D, Salvi R (2017) Effects of Cdh23 single nucleotide substitutions on age-related hearing loss in C57BL/6 and 129S1/Sv mice and comparisons with congenic strains. Sci Rep 7:44450.

Kato HK, Asinof SK, Isaacson JS (2017) Network-Level Control of Frequency Tuning in Auditory Cortex. Neuron.

Kato HK, Gillet SN, Isaacson JS (2015) Flexible Sensory Representations in Auditory Cortex Driven by Behavioral Relevance. Neuron 88:1027–1039.

Kuchibhotla KV, Gill JV, Lindsay GW, Papadoyannis ES, Field RE, Sten TAH, Miller KD, Froemke RC (2017) Parallel processing by cortical inhibition enables context-dependent behavior. Nature neuroscience 20:62–71.

Lee S, Hjerling-Leffler J, Zagha E, Fishell G, Rudy B (2010) The Largest Group of Superficial Neocortical GABAergic Interneurons Expresses Ionotropic Serotonin Receptors. J Neurosci 30:16796–16808.

Lesicko AMH, Angeloni CF, Blackwell JM, De Biasi M, Geffen MN (2022) Corticofugal regulation of predictive coding. Elife 11:e73289.

Levy RB, Reyes AD (2012) Spatial Profile of Excitatory and Inhibitory Synaptic Connectivity in Mouse Primary Auditory Cortex. Journal of Neuroscience 32:5609–5619.

Li LY, Xiong XR, Ibrahim LA, Yuan W, Tao HW, Zhang LI (2015) Differential Receptive Field Properties of Parvalbumin and Somatostatin Inhibitory Neurons in Mouse Auditory Cortex. Cerebral cortex 25:1782–1791.

Malmierca MS, Anderson LA, Antunes FM (2015) The cortical modulation of stimulus-specific adaptation in the auditory midbrain and thalamus: a potential neuronal correlate for predictive coding. Front Syst Neurosci 9:19.

Mehra M, Mukesh A, Bandyopadhyay S (2022) Separate Functional Subnetworks of Excitatory Neurons Show Preference to Periodic and Random Sound Structures. J Neurosci 42:3165–3183.

Mesik L, Ma W, Li L, Ibrahim LA, Huang ZJ, Zhang LI, Tao HW (2015) Functional response properties of VIP-expressing inhibitory neurons in mouse visual and auditory cortex. Front Neural Circuits 9:22.

Meyer HS, Schwarz D, Wimmer VC, Schmitt AC, Kerr JND, Sakmann B, Helmstaedter M (2011) Inhibitory interneurons in a cortical column form hot zones of inhibition in layers 2 and 5A. Proceedings of the National Academy of Sciences 108:16807–16812.

Millman DJ, Ocker GK, Caldejon S, Kato I, Larkin JD, Lee EK, Luviano J, Nayan C, Nguyen TV, North K, Seid S, White C, Lecoq J, Reid C, Buice MA, de Vries SE (2020) VIP interneurons in mouse primary visual cortex selectively enhance responses to weak but specific stimuli Vinck M, Wassum KM, eds. eLife 9:e55130.

Myers-Joseph D, Wilmes KA, Fernandez-Otero M, Clopath C, Khan AG (2024) Disinhibition by VIP interneurons is orthogonal to cross-modal attentional modulation in primary visual cortex. Neuron 112:628-645.e7.

Naatanen R, Gaillard AW, Mantysalo S (1978) Early selective-attention effect on evoked potential reinterpreted. Acta psychologica 42:313–329.

Naatanen R, Paavilainen P, Rinne T, Alho K (2007) The mismatch negativity (MMN) in basic research of central auditory processing: a review. Clin Neurophysiol 118:2544–2590.

Naatanen R, Pakarinen S, Rinne T, Takegata R (2004) The mismatch negativity (MMN): towards the optimal paradigm. Clin Neurophysiol 115:140–144.

Najafi F, Russo S, Lecoq J (2025) Unexpected events trigger task-independent signaling in VIP and excitatory neurons of mouse visual cortex. iScience 28:111728.

Naka A, Veit J, Shababo B, Chance RK, Risso D, Stafford D, Snyder B, Egladyous A, Chu D, Sridharan S, Mossing DP, Paninski L, Ngai J, Adesnik H (2019) Complementary networks of cortical somatostatin interneurons enforce layer specific control. Elife 8:e43696.

Natan RG, Briguglio JJ, Mwilambwe-Tshilobo L, Jones SI, Aizenberg M, Goldberg EM, Geffen MN (2015) Complementary control of sensory adaptation by two types of cortical interneurons. eLife 4:1–27.

Natan RG, Rao W, Geffen MN (2017) Cortical Interneurons Differentially Shape Frequency Tuning following Adaptation. Cell Reports 21:878–890.

Nelken I (2004) Processing of complex stimuli and natural scenes in the auditory cortex. Current opinion in neurobiology 14:474–480.

Nelken I (2014) Stimulus-specific adaptation and deviance detection in the auditory system: experiments and models. Biological cybernetics Available at: http://www.ncbi.nlm.nih.gov/pubmed/24477619.

Pachitariu M, Steinmetz N, Kadir S, Carandini M, D HK (2016) Kilosort: realtime spike-sorting for extracellular electrophysiology with hundreds of channels. :061481 Available at: https://www.biorxiv.org/content/10.1101/061481v1 [Accessed February 6, 2025].

Pachitariu M, Stringer C, Dipoppa M, Schröder S, Rossi LF, Dalgleish H, Carandini M, Harris KD (2017) Suite2p: beyond 10,000 neurons with standard two-photon microscopy. bioRxiv:061507.

Pakan JM, Lowe SC, Dylda E, Keemink SW, Currie SP, Coutts CA, Rochefort NL (2016) Behavioral-state modulation of inhibition is context-dependent and cell type specific in mouse visual cortex Mrsic-Flogel TD, ed. eLife 5:e14985.

Parras GG, Nieto-Diego J, Carbajal GV, Valdés-Baizabal C, Escera C, Malmierca MS (2017) Neurons along the auditory pathway exhibit a hierarchical organization of prediction error. Nat Commun 8:2148.

Paxinos G, Franklin KB (2012) The Mouse Brain in Stereotaxic Coordinates. Sydney: Academic Press.

Pfeffer CK, Xue M, He M, Huang ZJ, Scanziani M (2013) Inhibition of inhibition in visual cortex: the logic of connections between molecularly distinct interneurons. Nature neuroscience 16:1068–1076.

Phillips EA, Hasenstaub AR (2016) Asymmetric effects of activating and inactivating cortical interneurons. eLife 5 Available at: https://www.ncbi.nlm.nih.gov/pubmed/27719761.

Phillips EAK, Schreiner CE, Hasenstaub AR (2017) Cortical Interneurons Differentially Regulate the Effects of Acoustic Context. Cell Rep 20:771–778.

Pi HJ, Hangya B, Kvitsiani D, Sanders JI, Huang ZJ, Kepecs A (2013) Cortical interneurons that specialize in disinhibitory control. Nature 503:521–524.

Ramamurthy DL, Chen A, Zhou J, Park C, Huang PC, Bharghavan P, Krishna G, Liu J, Casale K, Feldman DE (2023) VIP interneurons in sensory cortex encode sensory and action signals but not direct reward signals. Current Biology 33:3398-3408.e7.

Romero S, Hight AE, Clayton KK, Resnik J, Williamson RS, Hancock KE, Polley DB (2020) Cellular and Widefield Imaging of Sound Frequency Organization in Primary and Higher Order Fields of the Mouse Auditory Cortex. Cerebral Cortex 30:1603–1622.

Rubin J, Ulanovsky N, Nelken I, Tishby N (2016) The Representation of Prediction Error in Auditory Cortex. PLoS Comput Biol 12:1005058.

Siegle JH, López AC, Patel YA, Abramov K, Ohayon S, Voigts J (2017) Open Ephys: an open-source, plugin-based platform for multichannel electrophysiology. J Neural Eng 14:045003.

Sohoglu E, Chait M (2016) Detecting and representing predictable structure during auditory scene analysis. eLife 5:1–17.

Solyga M, Keller GB (2025) Multimodal mismatch responses in mouse auditory cortex. eLife 13 Available at: https://elifesciences.org/reviewed-preprints/95398 [Accessed February 19, 2025].

Southwell R, Chait M (2018) Enhanced deviant responses in patterned relative to random sound sequences. Cortex 109:92–103.

Szymanski FD, Garcia-Lazaro JA, Schnupp JWH (2009) Current Source Density Profiles of Stimulus-Specific Adaptation in Rat Auditory Cortex. Journal of Neurophysiology 102:1483–1490.

Tobin M, Sheth J, Wood KC, Michel EK, Geffen MN (2024) Distinct inhibitory neurons differently shape neuronal codes for sound intensity in the auditory cortex. J Neurosci Available at: https://www.jneurosci.org/content/early/2024/11/06/JNEUROSCI.1502-23.2024 [Accessed December 16, 2024].

Tremblay R, Lee S, Rudy B (2016) GABAergic Interneurons in the Neocortex: From Cellular Properties to Circuits. Neuron 91:260–292.

Tsukano H, Garcia MM, Dandu PR, Kato HK (2025) Predictive filtering of sensory response via orbitofrontal top-down input. bioRxiv:2024.09.17.613562.

Ulanovsky N, Las L, Farkas D, Nelken I (2004) Multiple time scales of adaptation in auditory cortex neurons. Journal of Neuroscience 24:10440–10453.

Ulanovsky N, Las L, Nelken I (2003) Processing of low-probability sounds by cortical neurons. Nature Neuroscience 6:391–398.

Vapnik V (2013) The Nature of Statistical Learning Theory. Springer Science & Business Media.

Vogler NW, Chen R, Virkler A, Tu VY, Gottfried JA, Geffen MN (2024) Direct Piriform-to-Auditory Cortical Projections Shape Auditory–Olfactory Integration. J Neurosci 44 Available at: https://www.jneurosci.org/content/44/49/e1140242024 [Accessed February 6, 2025].

Wood KC, Angeloni CF, Oxman K, Clopath C, Geffen MN (2022) Neuronal activity in sensory cortex predicts the specificity of learning in mice. Nature Communications 13.

Wood KC, Blackwell JM, Geffen MN (2017) Cortical inhibitory interneurons control sensory processing. Current Opinion in Neurobiology 46:200–207.

Wu J, Zhao Z, Shi Y, He M (2022) Cortical VIP+ Interneurons in the Upper and Deeper Layers Are Transcriptionally Distinct. J Mol Neurosci 72:1779–1795.

Yarden TS, Mizrahi A, Nelken I (2022) Context-Dependent Inhibitory Control of Stimulus-Specific Adaptation. J Neurosci 42:4629–4651.

Yaron A, Hershenhoren I, Nelken I (2012) Sensitivity to Complex Statistical Regularities in Rat Auditory Cortex. Neuron 76:603–615.

Yavorska I, Wehr MS (2016) Somatostatin-Expressing Inhibitory Interneurons in Cortical Circuits. Frontiers in Neural Circuits 10:1–18.

843 **FIGURES**

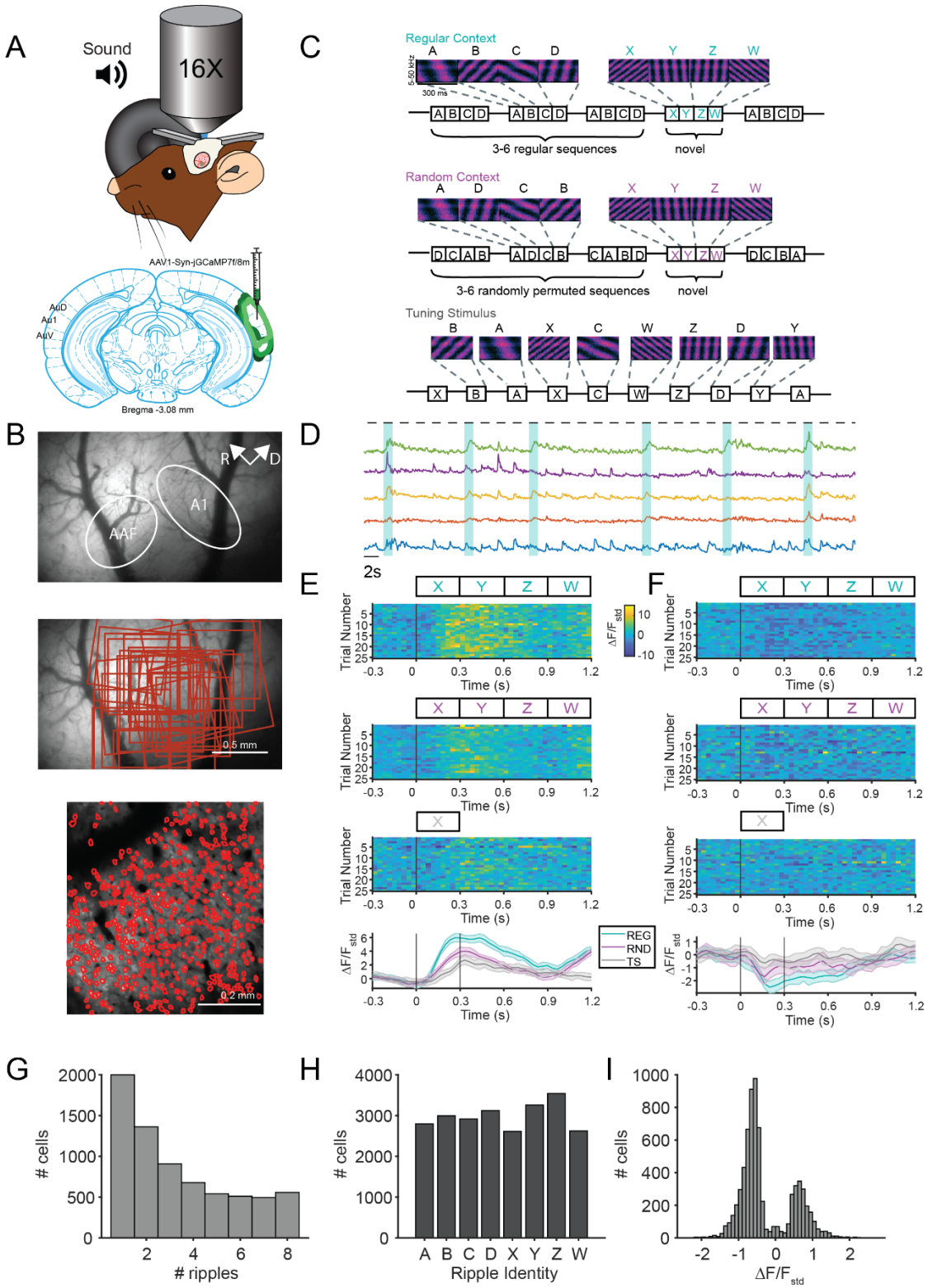

844

845 **Figure 1.**

846 **A.** Schematic of two-photon (2P) calcium imaging setup (top), and viral spread across AC for
847 GCaMP injections (bottom). **B.** Widefield image from an example mouse with estimated areas for
848 A1 and anterior auditory field (AAF) regions (top). Recording sites across different mice mapped
849 onto the example widefield image (middle). Example 2P imaging site with ROIs circled in red
850 (bottom). **C.** Spectrograms of spectro-temporal moving ripples used in the experiment and
851 stimulus schematic. Ripples spanned 5-50 kHz and were 300 ms long in duration. Regular
852 sequences had a fixed temporal pattern (ABCD ABCD…) while random sequences shuffled the
853 background ripple order (DCAB BACD…). The deviant stimulus (novel) sequence was the same
854 for both conditions (XYZW). Each letter in the diagram represents a different spectro-temporal
855 moving ripple. **D.** Example 2P calcium traces from 5 neurons from the same recording session.
856 Black bars on top denote the timing of each ripple sequence. Blue outlines denote the timing of
857 deviant ripple sequences. **E,F.** Responses over the successive trials (top 3 plots) and mean response
858 trace (bottom) to the same deviant ripple in regular (cyan) and random (magenta) contexts as well
859 as the same ripple in the tuning sequence (gray) from example cells with a positive response (**E**)
860 and a negative response (**F**). Shaded error bars represent SEM. **G.** Histogram of number of neurons
861 responsive to only 1 ripple up to all 8 ripples. A significant response was determined with a t-test
862 of the mean response from 0-300 ms post-stimulus a $p < 0.05$ with a Bonferroni correction. **H.**
863 Histogram of number of neurons responsive to specific ripples. **I.** Histogram of response strengths
864 in response to baseline moving ripples for all sound responsive neurons.

865

866

867

Figure 2

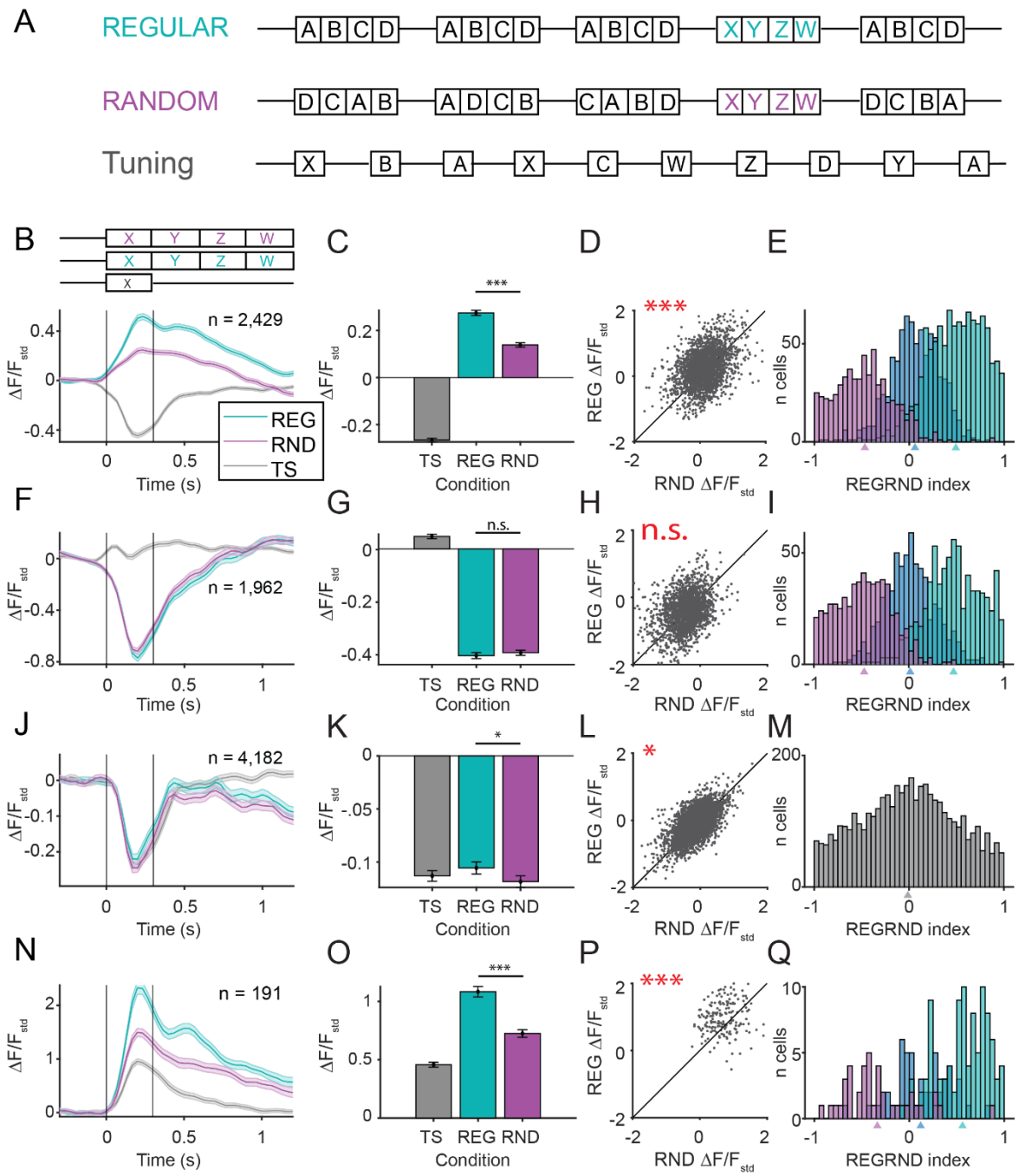

AC neurons exhibit stronger deviance responses in regular than random contexts.

A. Schematic of the stimuli for REG and RND contexts (sequence of 4 ripples ABCD) with deviant ripples (XYZW). A tuning stimulus comprising each of 8 ripples was used to identify the baseline

sound response to the ripples for individual neurons. **B.** Population-averaged calcium traces across neurons with positive deviance response to the deviant ripple presented in the REG context (cyan), RND context (magenta), and as part of tuning stimulus (grey) as z-scored ΔF/F on the left. Vertical lines represent duration of the first deviant ripple. **C.** Mean responses to the deviant ripple over 300 ms post stimulus onset in REG, RND and tuning (TS) contexts. **D.** Scatter plot of responses to deviant ripple under REG and RND contexts. **E.** Histogram of the REGRND index for responses to the deviant ripple for neurons with preference for REG context (cyan), RND context (magenta) or no preferences (gray). Mean values for the index for each group are denoted by triangles below the x-axis. **B, C, D, E.** Responses of neurons that exhibit positive responses to deviant ripple under either REG or RND contexts. The mean responses show a significant effect of context on the response amplitude ($n = 2{,}429$, lme, $p < 1e\text{-}20$) with deviance responses in REG context being the strongest (REG), followed by deviance responses in RND context (RND), and then the tuning stimulus responses (TS) (post-hoc Tukey-Kramer, $p = 5.96e\text{-}08$). **F, G, H, I.** Similar to B-E, but for responses of neurons that exhibit negative responses to deviant ripples under either REG or RND context ($n = 1{,}962$). For negative responses, there is no difference between REG and RND deviance responses (lme, n.s.). **J, K, L, M.** Similar to above, but for all neurons without a significant deviance response ($n = 4{,}182$, lme, n.s.). **N, O, P, Q.** Similar to above, for all neurons with both a positive sound response and a positive deviance response ($n = 191$, lme, $p = 4.11e\text{-}15$). REG responses are the strongest, followed by RND responses, followed by TS responses (post-hoc Tukey-Kramer, $p = 5.96e\text{-}8$).

Figure 3

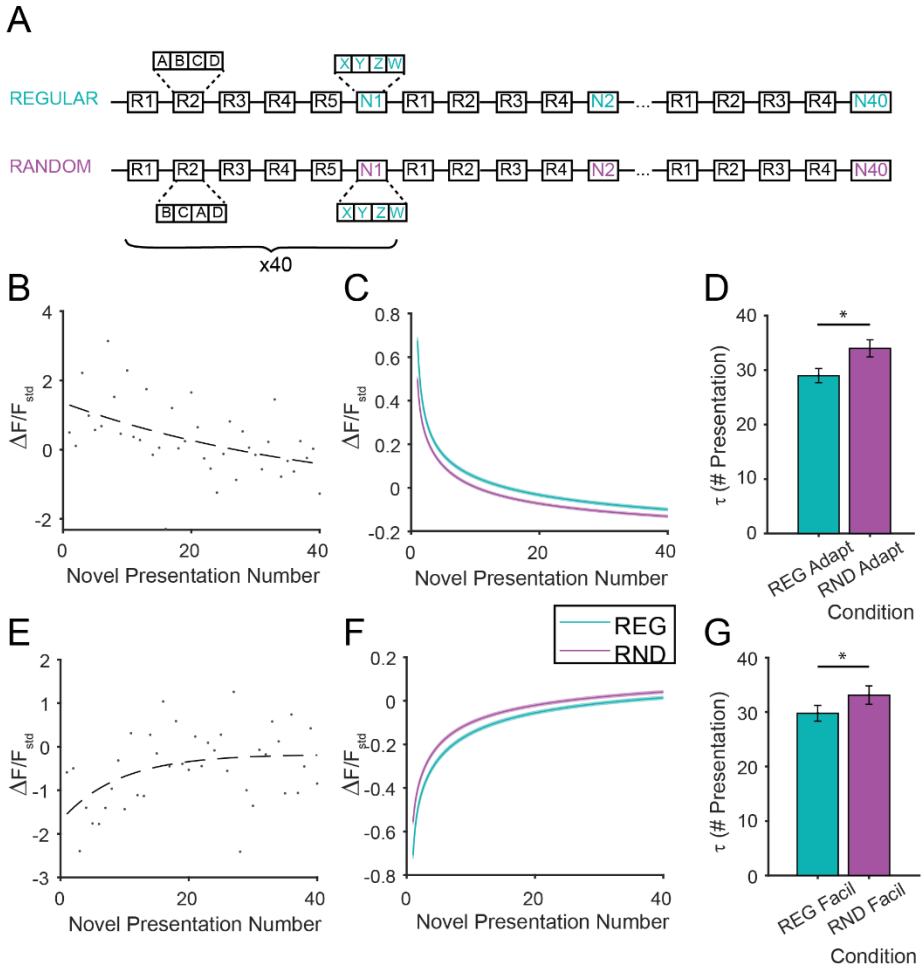

Temporal regularity modulates long-term deviance response dynamics.

A. Ripple sequences were presented in blocks of entire REG or RND contexts. The deviant ripple is always the same, allowing for potential adaptation to the deviant ripple itself. **B, E.** Deviance responses over successive deviant stimulus presentations, for example cells exhibiting adaptation (B) and facilitation (E) in neuronal responses to the deviant ripple sequence in a REG context. Dots denote response strength for a individual deviant ripple presentation and the dashed line is the best exponential fit. **C, F.** Exponential fits for adaptation (C) and facilitation (F) in REG (cyan) and RND (magenta) contexts across the population. **D, G.** Mean time constants for adaptation (D)

and facilitation (G) in REG and RND contexts for all neurons that exhibit such long-term dynamics. Both adaptation and facilitation are faster in the REG context (lower time constant, 2-way ANOVA, $p = 0.0044$).

Figure 4

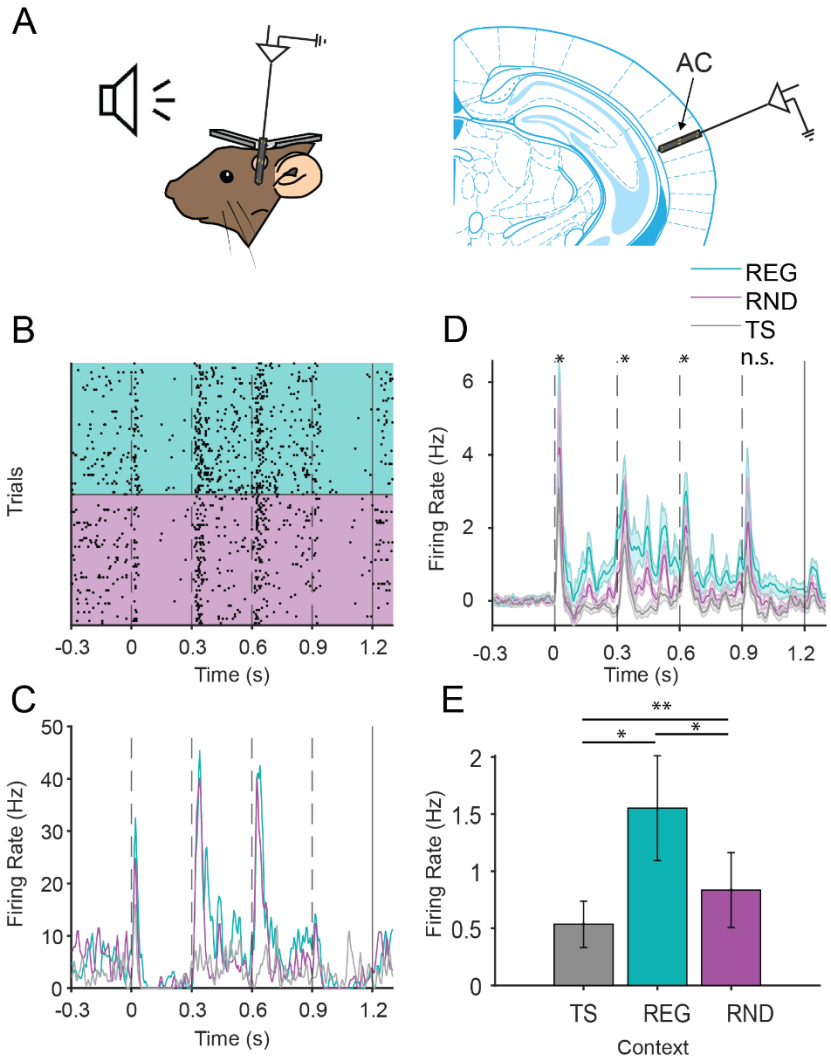

AC neurons exhibit higher firing rates to deviant ripples in regular as compared to random contexts.

A. Left: schematic of electrophysiological recordings from AC in awake head-fixed mice. Right: Electrode superimposed on the AC outline from the Paxinos Brain Atlas (Paxinos and Franklin, 2012). **B.** Raster plot of spike times from an example neuron in response to the deviant ripple sequence in REG (cyan) and RND (magenta) context. **C.** PSTH of the same neuron's firing rate in response to the deviant ripple sequence in REG and RND as well as the tuning response to the first

ripple in the deviant sequence (grey). **D.** Mean firing rates over all neurons with a significant deviance response (n = 164) to the deviant ripple sequence in REG (cyan), RND (magenta), and to the first ripple in isolation (grey). **E.** Mean firing rates in the first 100 ms post stimulus onset in REG, RND, and tuning contexts show a significant effect of context on deviant ripple responses (repeated measures ANOVA, $f(2) = 9.36$, $p = 0.00011$). Error bars represent SEM.

927 **Figure 5**

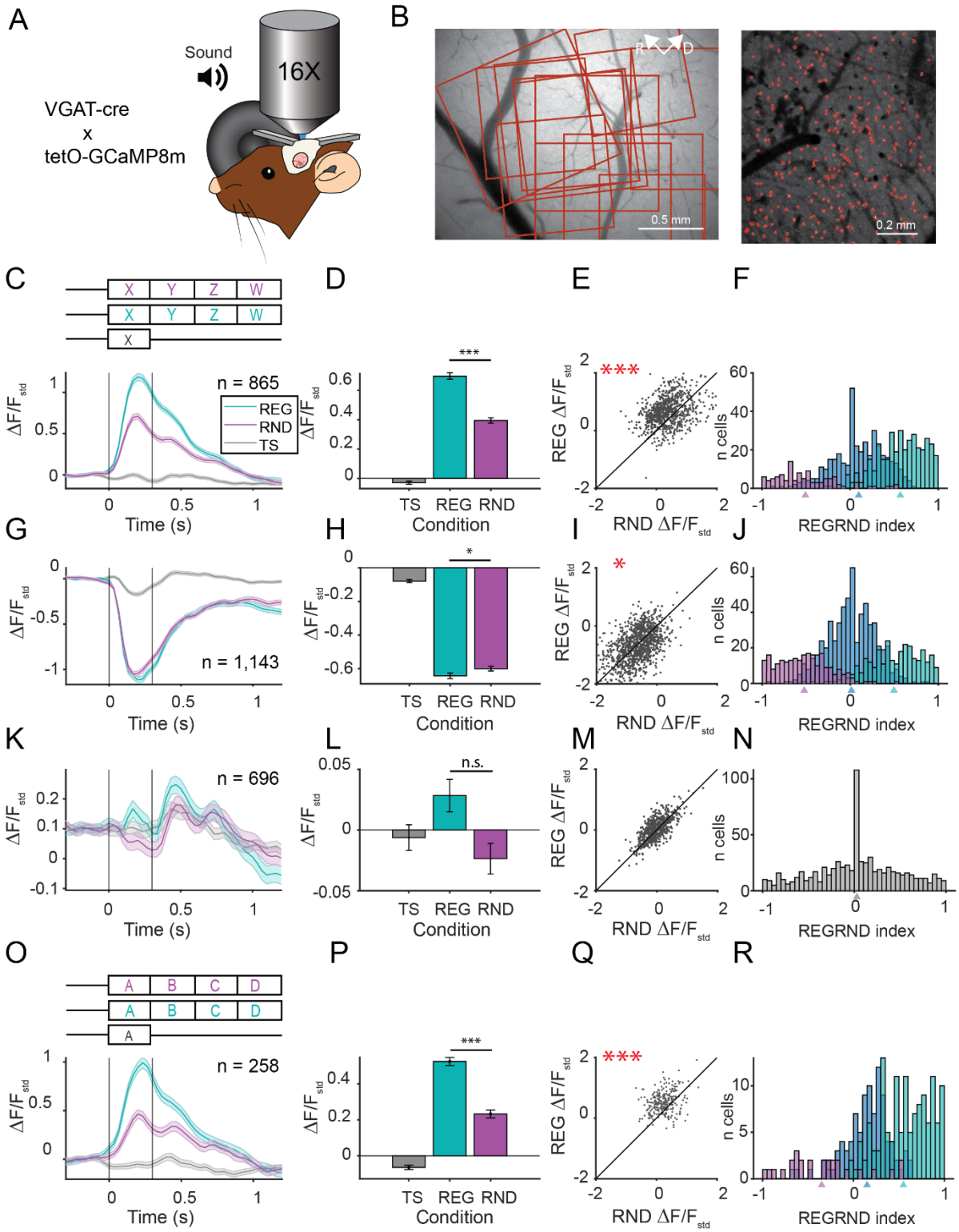

928

929 **Inhibitory neurons in AC exhibit context-dependent deviance responses.**

A. Schematic of 2-photon imaging from a transgenic mouse line expressing GCaMP8m only in inhibitory neurons. **B.** Left: Representative fields of view imaged (white boxes) overlayed on AC. For clarity, imaging areas close to one another have been combined. Right: representative field of view with identified neurons outlines using Suite2p. **C, G, K, O.** Population-averaged calcium traces across neurons with positive deviance response to the deviant ripple presented in the REG context (cyan), RND context (magenta), and as part of tuning stimulus (TS, grey) as z-scored ΔF/F on the left. Vertical lines represent duration of the first deviant ripple. **D, H, L, P.** Mean responses to the deviant ripple over 300 ms post stimulus onset in REG, RND and TS contexts. **E, I, M, Q.** Scatter plot of responses to the deviant ripple under REG and RND contexts. **F, J, N, R.** Histogram of the REGRND index for responses to the deviant ripple for neurons with preference for REG context (cyan), RND context (magenta) or no preferences (gray). Mean values for the index for each group are denoted by triangles below the x-axis. **C, D, E, F.** Responses to the deviant ripple over neurons with positive deviance responses (n = 865). REG deviance responses are significantly greater than RND deviance responses (lme, $p < 1e-20$). **G, H, I, J.** Similar to C-F, but for all negative deviance responses (n = 1,143). For negative responses, REG deviance responses were lower than RND responses (lme, $p= 0.046$). **K, L, M, N.** Similar to C-F, but for average responses of all neurons without a significant deviance response (n = 696). There is an increase in deviant responses in REG as compared to RND context (lme, $p = 0.011$). However, this was not significant in post-hoc Tukey-Kramer test. **O, P, Q, R.** Similar to C-F, but for recordings to stimuli in which background and deviant ripples were swapped (ABCD was the deviance sequence and XYZW was the background sequence) (n = 258, lme, $p < 1e-20$). Responses in REG context are the strongest, followed by responses in RND context, followed by TS responses (post-hoc Tukey-Kramer, $p = 1.19e-07$).

Figure 6

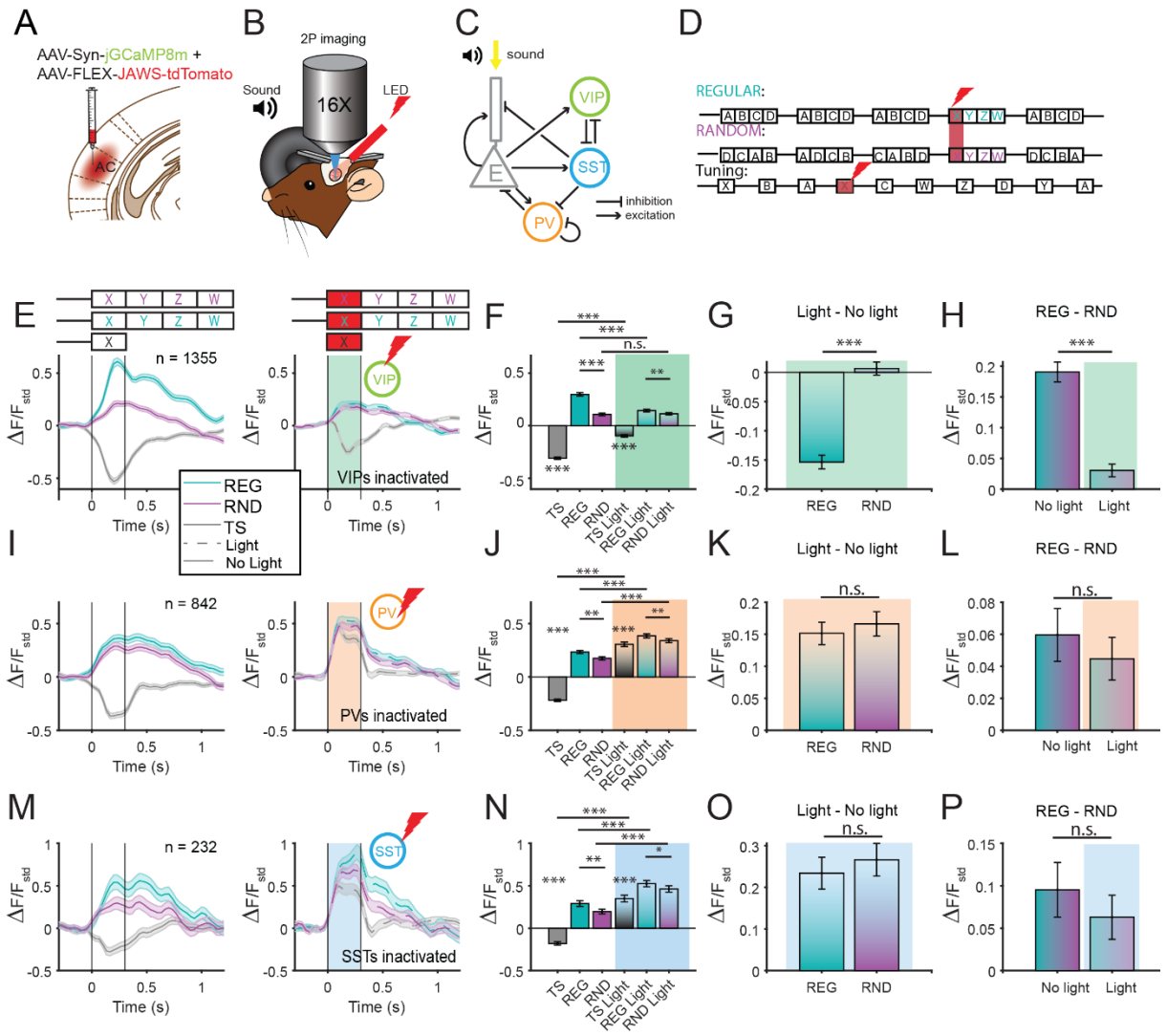

Selective context-dependent modulation of deviance responses by VIP neurons.

A, B, C, D. Schematics of the experimental set-up. **A.** Viral injection targeted to A1 included injection of a virus encoding GCaMP and a virus encoding a JAW-tdTomato construct in a Cre-dependent fashion into VIP-Cre, PV-Cre, or SST-Cre mice. Image from the Paxinos Brain atlas (Paxinos and Franklin, 2012). **B.** 2P imaging was performed in mice injected with JAWS-tdTomato

961 in addition to GCaMP. **C.** Simplified diagram of the inhibitory-excitatory microcircuit in A1 that
962 includes PV, SST and VIP neurons. PV neurons largely target the excitatory neuronal cell bodies,
963 SST neurons target distal dendrites, whereas the VIP neurons inhibit SST neurons. **D.** Diagram of
964 the stimulus with the light delivered during the deviant stimulus presentation on a subset of trials.
965 Optogenetic inactivation was performed during the first ripple in the deviant sequence. **E, I, M.**
966 Population-averaged calcium traces across neurons with positive deviance responses to the deviant
967 ripple presented in the REG context (cyan), RND context (magenta), and as part of tuning stimulus
968 (grey) as z-scored ΔF/F. Left: light off; Right: light on. Vertical lines represent duration of the first
969 deviant ripple. **F, J, N.** Mean responses to deviant ripple over 300 ms post stimulus onset in REG,
970 RND and TS contexts. Left: light off. Right: Light on. **G, K, O.** Mean changes in deviance
971 responses due to inactivation of inhibitory neurons under REG (cyan) and RND (magenta)
972 contexts. **H, L, P.** Mean difference in deviance responses between REG and RND contexts without
973 light (left) and with light (during inhibitory neuron inactivation, right). **E, F, G, H.** Effects of
974 inactivation of VIP inhibitory neurons. Inactivation of VIP neurons reduces the deviance response
975 (n = 1,355, linear mixed effects model, p = 5.02e-19). This modulation of the deviance response
976 is context-specific, with a much larger reduction in deviance responses under REG as compared
977 to RND context (linear mixed effects model, interaction term, p = 4.48e-11). **I, J, K, L.** Effects of
978 inactivation of PV inhibitory neurons. Inactivation of PV neurons increases the deviance response
979 (n = 842, linear mixed effects model, p = 2.86e-11) and does not result in a differential effect of
980 context (linear mixed effects model, interaction term, p = 0.64). **M, N, O, P.** Effects of inactivation
981 of SST inhibitory neurons. Optogenetic inactivation of SST cells also increases the deviance
982 response (n = 232, linear mixed effects model, p = 1.1e-6) but does not result in a significant
983 differential effect of context (linear mixed effects model, interaction term, p = 0. 63).

Figure 7

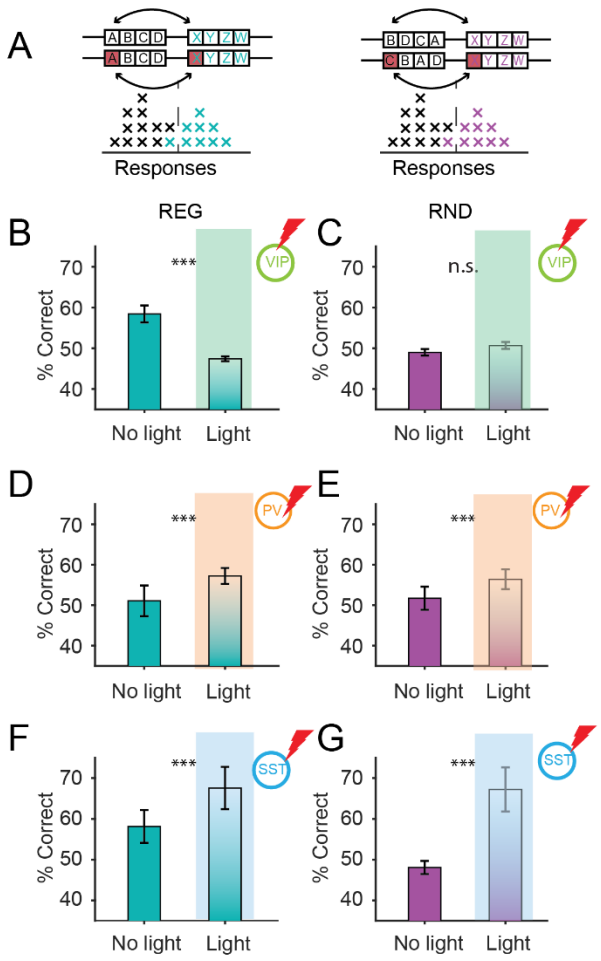

Differential effect of inhibitory neuronal inactivation on deviance detection under random and regular contexts.

A. Schematic of SVM classification for single neuronal responses to deviant and context ripples. The activity during individual presentations of the context ripple and the deviant ripple X was used to train the classifier under REG and RND contexts and during light and no light trials. **B-G.** Single neuron SVM performance for trials with (left) and without (right) light in the REG (B, D, F) and RND (C, E, G) contexts. **B, C.** VIP inactivation decreases SVM performance in REG context (post-

994 hoc Tukey-Kramer, $p = 0.00036$), but not in RND context (post-hoc Tukey-Kramer, $p = 0.85$). **D,**
995 **E.** PV inactivation improves SVM performance in REG context (post-hoc Tukey-Kramer, $p <$
996 $7.76e-7$) and in RND context (post-hoc Tukey-Kramer, $p = 0.00017$). **F, G.** SST inactivation
997 improves SVM performance in REG context (post-hoc Tukey-Kramer, $p < 1.28e-7$) and in RND
998 context (post-hoc Tukey-Kramer, $p < 4.98e-9$).

999

1000

Figure 8

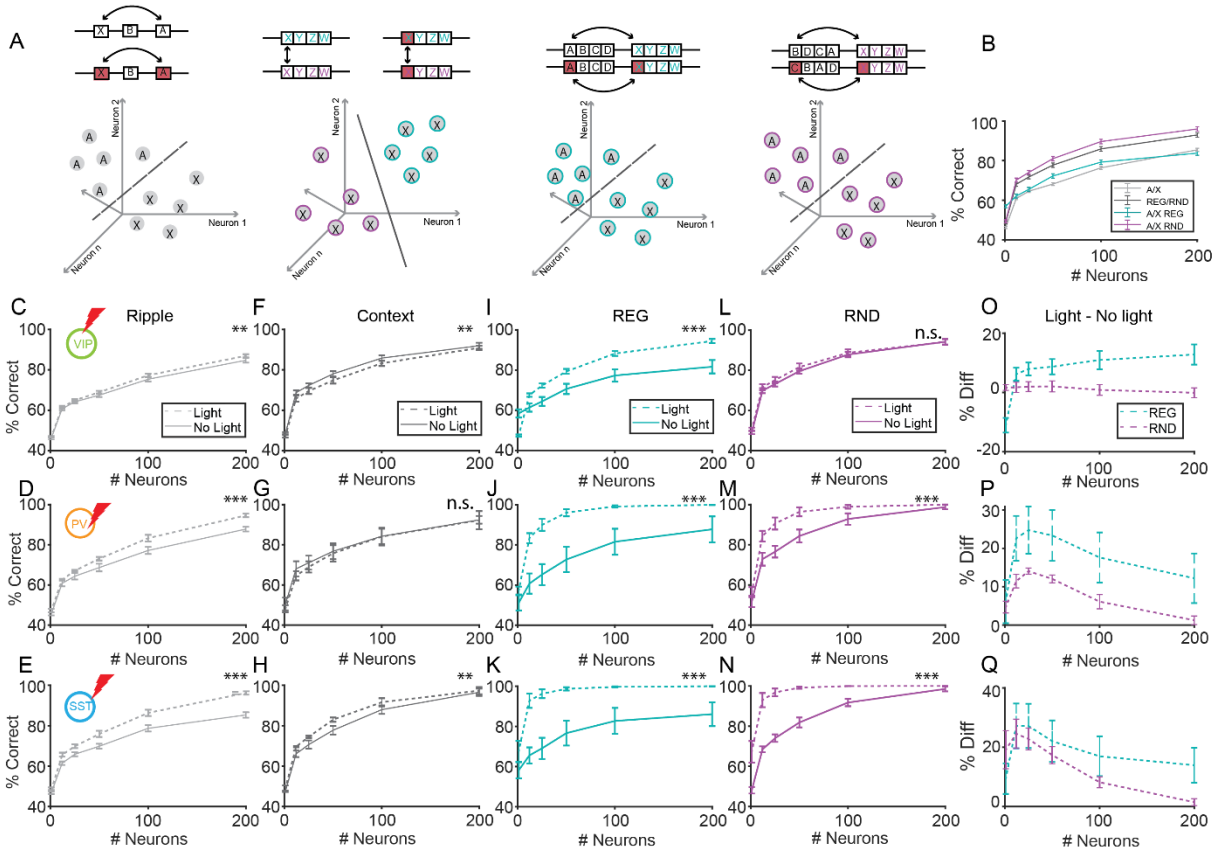

Deviance decoding is improved with inhibitory neuron inactivation at the population level. **A.** Schematic of a SVM identifying a linear decision boundary between points in a high dimensional space. We computed the SVM to discriminate between ripples A and X from the tuning response stimulus; for the deviant ripple X under REG and RND contexts; for the deviant ripple X versus background context ripple under REG; and RND contexts. All SVMs were trained and tested on data with and without optogenetic inactivation for each of the three inhibitory neuronal classes. **B.** SVM discrimination performance between context ripple and deviant ripple X from the sound response stimulus (grey); discrimination performance of the deviant ripple X between REG and RND contexts using the deviance response (black); deviance detection of X under REG (cyan) and RND (magenta) contexts. Context is easier to classify than ripple identity

(2-way ANOVA, f(1)=196.25, p=9.38e-33). **C, D, E.** Effect of optogenetic inactivation of VIP (C), PV (D), and SST (E) neurons on ripple discrimination. Here and below, lines represent classifier performance; solid: trials without light; dashed: trials with light. Inactivation of VIP (2-way ANOVA, f(1) = 7.45, p = 0.0072), PV (2-way ANOVA, f(1) = 27.50, p = 5.094e-6), and SST (2-way ANOVA, f(1) = 58.62, p = 1.98e-9) neurons all improved ripple discrimination performance. **F, G, H.** Effects of inactivation of VIP (F), PV (G), and SST (H) neurons on discrimination of deviant ripple X under REG versus RND contexts. VIP inactivation decreased classification performance (2-way ANOVA, f(1) = 10.058, p = 0.0019) while SST inactivation improved performance (2-way ANOVA, f(1) = 12.47, p = 0.001), and PV inactivation did not have a significant effect (2-way ANOVA, f(1) = 0.67, p = 0.42). **I, J, K.** Effects of inactivation of VIP (I), PV (J), and SST (K) neurons on discriminating background and deviant ripples under the REG context. All inactivations improved performance: PV (2-way ANOVA, f(1) = 50.18, p = 1.26e-8); SST (2-way ANOVA, f(1) = 58.45, p = 2.05e-9); VIP (2-way ANOVA, f(1) = 20.54, p = 1.26e-5) neuronal inactivation. **L, M, N.** Effects of inactivation of VIP (L), PV (M), and SST (N) neurons on discriminating background and deviant ripples in the RND context. Both PV (2-way ANOVA, f(1) = 29.35, p = 2.91e-6) and SST neuronal inactivation (2-way ANOVA, f(1) = 75.31, p = 7.93e-9) enhanced performance, while VIP neuronal inactivation had no effect on classification performance (2-way ANOVA, f(1) = 3.02, p = 0.085). **O, P, Q.** Difference between classification performance with and without light inactivation for corresponding panels I-N. VIP inactivation (2-way ANOVA, f(1) = 9.8941, p = 0.0020) and PV inactivation (2-way ANOVA, f(1) = 14.407, p = 0. 0048) had significant differences in their effects on SVM discrimination performance across REG and RND contexts while SST inactivation did not (2-way ANOVA, f(1) = 1.5055, p = 0.23).

1036 **Table 1.**

Comparison	Figure	Test	N	Statistic	Effect Size	p-value
ANOVA for effects of REG/RND context on deviance response, all positive deviance responses	2b	One-way repeated measures ANOVA	2429	F(2)=1816.91	η2=0.428	<1e-20
Multiple comparison for REG, RND, and base sound response, all positive deviance responses	2c,d	post-hoc Tukey-Kramer	2429	MeanDifferenceBASEREG=-0.541 MeanDifferenceBASERND=-0.404 MeanDifferenceREGRND=0.136	n/a	5.96e-08 5.96e-08 5.96e-08
REGRND index for neurons responsive to both contexts, positive deviance	2e	t-test	769	Mean=0.0602	n/a	1.31e-10
Effect of Regularity on Novelty Responses, positive novelty responses	2b-d	Linear mixed effects model	2429	F(1, 7284) = 121.761	0.136	<1e-20
Effect of Novelty in Regular Contex, positive novelty responses	2b-d	Linear mixed effects model	2429	F(1, 7284) = 1922.243	0.541	<1e-20
Effect of Novelty in Random Context, positive novelty responses	2b-d	Linear mixed effects model	2429	F(1, 7284) = 1076.42	0.404	<1e-20
ANOVA for effects of REG/RND context on deviance response, all negative deviance responses	2f	One-way repeated measures ANOVA	1962	F(2)=1324	η2=0.403	<1e-20
Multiple comparison for REG, RND, and base sound response, all negative deviance responses	2g,h	post-hoc Tukey-Kramer	1962	MeanDifferenceBASEREG=0.48 MeanDifferenceBASERND=0.464 MeanDifferenceREGRND=-0.0115	n/a	5.96e-08 5.96e-08 0.63
REGRND index for neurons responsive to both contexts, negative deviance	2i	t-test	634	Mean=0.0154	n/a	0.14
Effect of Regularity on Novelty Responses, negative novelty responses	2f-h	Linear mixed effects model	1662	F(1, 5883) = 0.719	-0.011	0.397
Effect of Novelty in Regular Contex, negative novelty responses	2f-h	Linear mixed effects model	1662	F(1, 5883) = 1227.638	-0.475	<1e-20
Effect of Novelty in Random Context, negative novelty responses	2f-h	Linear mixed effects model	1662	F(1, 5883) = 1168.945	-0.464	<1e-20
ANOVA for effects of REG/RND context on deviance response, all non-significant deviance responses	2j	One-way repeated measures ANOVA	4182	F(2)=3.8	η2=0.0009	0.023
Multiple comparison for REG, RND, and base sound response, all non-significant deviance responses	2k,l	post-hoc Tukey-Kramer	4182	MeanDifferenceBASEREG=-0.0075 MeanDifferenceBASERND=0.0053 MeanDifferenceREGRND=0.013	n/a	0.21 0.46 0.032
Effect of Regularity on Novelty Responses,	2j-l	Linear mixed	4182	F(1, 12543) = 2.965	0.013	0.0851

not significant novelty responses		effects model				
Effect of Novelty in Regular Contex, not significant novelty responses	2j-l	Linear mixed effects model	4182	F(1, 12543) = 1.012	0.007	0.314
Effect of Novelty in Random Context, not significant novelty responses	2j-l	Linear mixed effects model	4182	F(1, 12543) = 0.512	-0.005	0.474
ANOVA for effects of REG/RND context on deviance response, positive deviance and sound response	2n	One-way repeated measures ANOVA	191	F(2)=129.72	η2=.4057	1.14e-43
Multiple comparison for REG, RND, and base sound response, positive deviance and sound response	2o,p	post-hoc Tukey-Kramer	191	MeanDifferenceBASEREG=-0.625 MeanDifferenceBASERND=-0.268 MeanDifferenceREGRND=0.358	n/a	5.96e-08 5.96e-08 5.96e-08
REGRND index for neurons responsive to both contexts, positive deviance and sound response	2q	t-test	51	Mean=12	n/a	0.0046
Effect of Regularity on Novelty Responses, positive novelty responses	2n-p	Linear mixed effects model	191	F(1, 570) = 65.161	0.358	4.11e-15
Effect of Novelty in Regular Contex, positive novelty responses	2n-p	Linear mixed effects model	191	F(1, 570) = 199.046	0.625	<1e-20
Effect of Novelty in Random Context, positive responses	2n-p	Linear mixed effects model	191	F(1, 570) = 36.435	0.268	2.85E-09
ANOVA for effects of REG/RND context and adaptation/facilitation on time constants	3d,g	Two-way ANOVA	8644	FREGRND(1)=8.1256 Fadaptfacil(1)=5.57e-6	η2=9.39e-4 η2=6.45e-10	0.0044 0.99
Difference in response to second deviant ripple, first 100 ms	4d	paired t-test	164	MeanDifference=1.379	n/a	0.017
Difference in response to third deviant ripple, first 100 ms	4d	paired t-test	164	MeanDifference=0.952	n/a	0.019
Difference in response to fourth deviant ripple, first 100 ms	4d	paired t-test	164	MeanDifference=1.136	n/a	0.093
ANOVA for effect of context in deviance response for ephys	4e	repeated-measures anova	164	F(2)=9.3602	η2=0.0099598	0.00011
Multiple comparison for REG, RND, and base sound response, ephys	4e	post-hoc Tukey-Kramer	164	MeanDifferenceREGRND=0.0102 MeanDifferenceREGBASE=0.0153 MeanDifferenceRNDBASE=0.00507	n/a	0.024 0.0022 0.0091
ANOVA for effects of REG/RND context on deviance response, all positive deviance responses	5c	One-way repeated measures ANOVA	865	F(2)=79.10	η2=0.4441	5.64e-26
Multiple comparison for REG, RND, and base sound response, all positive deviance responses	5d,e	post-hoc Tukey-Kramer	865	MeanDifferenceBASEREG=-0.572 MeanDifferenceBASERND=-0.323 MeanDifferenceREGRND=0.249	n/a	1.19e-07 1.19e-07 3.83e-05
REGRND index for neurons responsive to	5f	t-test	865	Mean=0.0984	n/a	1.31e-10

both contexts, positive deviance						
Effect of Regularity on Novelty Responses, positive novelty responses	5c-f	Linear mixed effects model	865	F(1, 2592) = 152.299	0.261	<1e-20
Effect of Novelty in Regular Contex, positive novelty responses	5c-f	Linear mixed effects model	865	F(1, 2592) = 991.339	0.666	<1e-20
Effect of Novelty in Random Context, positive novelty responses	5c-f	Linear mixed effects model	865	F(1, 2592) = 366.515	0.405	<1e-20
ANOVA for effects of REG/RND context on deviance response, all negative deviance responses	5c-f	One-way repeated measures ANOVA	1143	F(2)=161.44	η2=0.6199	2.59e-42
Multiple comparison for REG, RND, and base sound response, all negative deviance responses	5h,i	post-hoc Tukey-Kramer	1143	MeanDifferenceBASEREG=0.72 MeanDifferenceBASERND=0.498 MeanDifferenceREGRND=-0.221	n/a	1.19e-07 1.19e-07 1.85e-06
REGRND index for neurons responsive to both contexts, negative deviance	5j	t-test	609	Mean=0.0124	n/a	0.25
Effect of Regularity on Novelty Responses, negative novelty responses	5g-i	Linear mixed effects model	1143	F(1, 3426) = 3.99	-0.036	0.0458
Effect of Novelty in Regular Contex, negative novelty responses	5g-i	Linear mixed effects model	1143	F(1, 3426) = 993.235	-0.561	<1e-20
Effect of Novelty in Random Context, negative novelty responses	5g-i	Linear mixed effects model	1143	F(1, 3426) = 871.32	-0.526	<1e-20
ANOVA for effects of REG/RND context on deviance response, all non-significant deviance responses	5k	One-way repeated measures ANOVA	696	F(2)=0.02	η2=0.0002115	0.98
Multiple comparison for REG, RND, and base sound response, all non-significant deviance responses	5l,m	post-hoc Tukey-Kramer	696	MeanDifferenceBASEREG=-0.00199 MeanDifferenceBASERND=-0.00476 MeanDifferenceREGRND=-0.00277	n/a	0.99 0.98 0.99
Effect of Regularity on Novelty Responses, not significant novelty responses	5k-n	Linear mixed effects model	696	F(1, 2085) = 6.537	0.042	0.0106
Effect of Novelty in Regular Contex, not significant novelty responses	5 k-n	Linear mixed effects model	696	F(1, 2085) = 2.908	0.028	0.0883
Effect of Novelty in Random Context, not significant novelty responses	5 k-n	Linear mixed effects model	696	F(1, 2085) = 0.725	-0.014	0.395
ANOVA for effects of REG/RND context on deviance response, all positive deviance responses, swapped ripples	5o	One-way repeated measures ANOVA	258	F(2)=172.25	η2=0.635	4.62e-44

Multiple comparison for REG, RND, and base sound response, all positive deviance responses, swapped ripples	5p,q	post-hoc Tukey-Kramer	258	MeanDifferenceBASEREG=-0.631 MeanDifferenceBASERND=-0.295 MeanDifferenceREGRND=0.336	n/a	1.19e-07 1.19e-07 1.19e-07
REGRND index for neurons responsive to both contexts, positive deviance, swapped ripples	5r	t-test	258	Mean=0.154	n/a	7.02e-09
Effect of Regularity on Novelty Responses, positive novelty responses	5o-q	Linear mixed effects model	258	F(1, 771) = 112.939	0.292	<1e-20
Effect of Novelty in Regular Contex, positive novelty responses	5o-q	Linear mixed effects model	258	F(1, 771) = 459.732	0.588	<1e-20
Effect of Novelty in Random Context, positive responses	5o-q	Linear mixed effects model	258	F(1, 771) = 116.944	0.297	<1e-20
LME for effects of context and optogenetic inactivation of VIPs on deviance responses	6e,f,g,h	Linear mixed effects model	1355	F(1,5416)LIGHT=36.60 F(1,5416)REGRND=82.96 F(1,5416)Interaction=43.57	LIGHT= -0.073 REGRND=0.22 Interaction= 0.16	1.55e-09 1.16e-19 4.48e-11
LME contrasts, REG, RND, and base sound response, VIP optogenetic inactivation	6f	Linear mixed effects model	1355	F(1,5416)RNDLIGHTNOLIGHT=0.15 F(1,5416)REGLIGHTNOLIGHT= 80.01 F(1,5416)LIGHTREGRND= 123.39 F(1,5416)NOLIGHTREGRND=3.14	RNDLNL = 0.007 REGLNL = -0.15 LIGHTRR = 0.030 NOLIGHTRR = 0.19	0.697 5.02e-19 0.0763 2.32e-28
Baseline sound response, VIP inactivation	6f	t-test	1355	MeanNOLIGHT=-0.309 MeanLIGHT=-0.097	n/a	<1e-20 2.29e-17
Effect of inactivation of VIPs on baseline sound response	6f	paired t-test	1355	MeanDifference=-0.213	n/a	<1e-20
LME for effects of context and optogenetic inactivation of PVs on deviance responses	6i,j,k,l	Linear mixed effects model	842	F(1, 3364)LIGHT=98.12 F(1, 3364)REGRND=10.57 F(1, 3364)Interaction=0.22	LIGHT= -0.073 REGRND=0.22 Interaction= 0.16	8.07e-23 0.0012 0.64
LME contrasts, REG, RND, and base sound response, PV optogenetic inactivation	6j	Linear mixed effects model	842	F(1, 3364)RNDLIGHTNOLIGHT= 53.762 F(1, 3364)REGLIGHTNOLIGHT= 44.571 F(1, 3364)LIGHTREGRND= 3.885 F(1, 3364)NOLIGHTREGRND=6.90	RNDLNL = 0.17 REGLNL = -0.15 LIGHTRR = 0.045 NOLIGHTRR = 0.060	2.82e-13 2.86e-11 0.049 0.0087
Baseline sound response, PV inactivation	6j	t-test	842	MeanNOLIGHT=-0.219 MeanLIGHT=0.305	n/a	<1e-20 1.48e-42
Effect of inactivation of PVs on baseline sound response	6j	paired t-test	842	MeanDifference=-0.524	n/a	<1e-20
LME for effects of context and optogenetic	6m,n,o,p	Linear mixed effects model	232	F(1, 924)LIGHT=55.02 F(1, 924)REGRND=5.50 F(1, 924)Interaction=0.23	LIGHT=0.25 REGRND=0.08	2.7e-13 0.019 0.63

inactivation of SSTs on deviance responses					Interaction= 0.032	
LME contrasts, REG, RND, and base sound response, SST optogenetic inactivation	6n	Linear mixed effects model	232	F(1, 924)RNDLIGHTNOLIGHT=31.18 F(1, 924)REGLIGHTNOLIGHT= 24.0 F(1, 924)LIGHTREGRND= 1.74 F(1, 924)NOLIGHTREGRND=3.99	RNDLNL = 0.27 REGLNL =0.23 LIGHTRR = 0.063 NOLIGHTRR = 0.10	3.1e-08 1.1e-06 0.19 0.046
Baseline sound response, SST inactivation	6n	t-test	232	MeanNOLIGHT=-0.18 MeanLIGHT=0.349	n/a	9.27e-17 4.23e-16
Effect of inactivation of SSTs on baseline sound response	6n	paired t-test	232	MeanDifference=-0.529	n/a	4.19e-29
Cross session comparison of laser effect difference in REG and RND contexts by strain	6	Linear mixed effects model	nVIP= 1355 nPV=8 42 nSST= 232	F(1, 2426)VIP=31.953 F(1,2426)PV=0.339 F(1.2426)SST=0.653	VIP=0.16 PV=0.019 SST=0.037	1.76e-8 0.56 0.42
Pair comparison of laser effect difference in REG and RND contexts by strain	6	Linear mixed effects model	2429	F(1, 2426)VIPxPV= 7.13 F(1,2426) VIPxSST = 7.95 F(1.2426) SSTxPV =0.083	VIPxPV=0.15 VIPxSST=0.0 13 SSTxPV =0.017	0.0077 0.0049 0.77
Multiple comparisons for SVM classification on REG background vs REG deviant effects of light and population size with VIP inactivation	7b	post-hoc Tukey-Kramer	12	MeanDifference=-5.911	n/a	0.00036
Multiple comparisons for SVM classification on RND background vs RND deviant effects of light and population size with VIP inactivation	7c	post-hoc Tukey-Kramer	12	MeanDifference=-1.359	n/a	0.85
Multiple comparisons for SVM classification on REG background vs REG deviant effects of light and population size with PV inactivation	7d	post-hoc Tukey-Kramer	12	MeanDifference=-17.769	n/a	7.76e-07
Multiple comparisons for SVM classification on RND background vs RND deviant effects of light and population size with PV inactivation	7e	post-hoc Tukey-Kramer	12	MeanDifference=-8.257	n/a	0.00017
Multiple comparisons for SVM classification on REG background vs REG deviant effects of light and population size with SST inactivation	7f	post-hoc Tukey-Kramer	12	MeanDifference=-19.456	n/a	1.28e-07
Multiple comparisons for SVM classification on RND background vs RND deviant effects of light and population	7g	post-hoc Tukey-Kramer	12	MeanDifference=-15.581	n/a	4.98e-9

size with SST inactivation						
ANOVA for SVM classification performance on context and ripple identity	8b	2-way anova	20	Fpopsize(5)=519.13 Fcontextripple(1)=196.25	η2=0.86 η2=0.065	4.12e-124 9.38e-33
ANOVA for SVM classification performance on background and deviant in REG vs RND contexts	8b	2-way anova	20	Fpopsize(5)=106.91 Fregrnd1)=41.371	η2=0.66 η2=0.051	2.70e-58 7.070e-10
Multiple comparisons for SVM classification REG vs RND no light	8b	post-hoc Tukey-Kramer	20	MeanDifference=-6.7395	n/a	7.30e-09
ANOVA for SVM performance on ripple identity in VIP mice	8c	2-way anova	12	Fpopsize(5)=548.12 Flightnolight(1)=7.4468	η2=0.95 η2=0.0026	1.077e-88 0.0072
ANOVA for SVM performance on ripple identity in PV mice	8d	2-way anova	4	Fpopsize(5)=284.2 Flightnolight(1)=27.503	η2=0.95 η2=0.0185	1.11e-30 5.094e-06
ANOVA for SVM performance on ripple identity in SST mice	8e	2-way anova	4	Fpopsize(5)=261.82 Fclass(1)=58.62	η2=0.929 η2=0.0291	5.66-30 1.98e-09
ANOVA for SVM performance on context identity in VIP mice	8f	2-way anova	12	Fpopsize(5)=296.12 Fclass(1)=10.058	η2=0.910 η2=0.0062	1.39e-71 0.0019
ANOVA for SVM performance on context identity in PV mice	8g	2-way anova	4	Fpopsize(5)=42.809 Fclass(1)=0.67358	η2=0.837 η2=0.0026	3.17e-15 0.42
ANOVA for SVM performance on context identity in SST mice	8h	2-way anova	4	Fpopsize(5)=258.65 Fclass(1)=12.465	η2= 0.960 η2=0.0093	7.21e-30 0.0010
ANOVA for SVM performance on background vs deviant in REG in VIP mice	8i	2-way anova	12	Fpopsize(5)= 64.1 Fclass(1)=20.543	η2=0.671 η2=0.0430	3.45e-34 1.26e-05
ANOVA for SVM performance on background vs deviant in REG in PV mice	8j	2-way anova	4	Fpopsize(5)=22.11 Fclass(1)=50.178	η2=0.548 η2=0.249	1.12e-10 1.26e-08
ANOVA for SVM performance on background vs deviant in REG in SST mice	8k	2-way anova	4	Fpopsize(5)=12.54 Fclass(1)=58.452	η2= 0.387 η2=0.361	2.056e-07 2.054e-09
ANOVA for SVM performance on background vs deviant in RND in VIP mice	8l	2-way anova	12	Fpopsize(5)=265.13 Fclass(1)=3.016	η2=0.91 η2=0.0021	1.35e-68 0.085
ANOVA for SVM performance on background vs deviant in RND in PV mice	8m	2-way anova	4	Fpopsize(5)=77.016 Fclass(1)=29.35	η2=0.85 η2=0.064	9.49e-20 2.90e-06
ANOVA for SVM performance on background vs deviant in RND in SST mice	8n	2-way anova	4	Fpopsize(5)=46.278 Fclass(1)=75.309	η2= 0.67 η2=0.26	8.36e-16 7.92e-11
ANOVA for SVM performance difference on background vs deviant in REG/RND in VIP mice	8o	2-way anova	24	Fpopsize(5)=5.5069 Fclass(1)=9.8941	η2=0.16 η2=0.057	0.00012 0.0020
ANOVA for SVM performance difference on background vs	8p	2-way anova	8	Fpopsize(5)=3.7646 Fclass(1)=14.407	η2=0.25 η2=0.19	0.0068 0.00048

deviant in REG/RND in PV mice						
ANOVA for SVM performance difference on background vs deviant in REG/RND in SST mice	8q	2-way anova	8	Fpopsize(5)= 3.4993 Fclass(1)= 1.5055	η2= 0.29 η2=0.025	0.010 0.23
Effect of regularity in pos novelty responses in VIP-cre recordings	S4a	Linear mixed effects model	648	F(1,1294)=103.96	β=-0.33,SE=0.03	1.56e-23
Effect of regularity in pos novelty responses in PV-cre recordings	S4c	Linear mixed effects model	350	F(1,698)=16.263	β=-0.16,SE=0.04	6.12e-5
Effect of regularity in pos novelty responses in SST-cre recordings	S4e	Linear mixed effects model	107	F(1,212)=11.398	β=-0.27,SE=0.08	0.00087
Effect of regularity in neg novelty responses in VIP-cre recordings	S4b	Linear mixed effects model	519	F(1,1036)=0.9849	β=-0.037,SE=0.038	0.32
Effect of regularity in neg novelty responses in PV-cre recordings	S4d	Linear mixed effects model	274	F(1,546)=1.9506	β=-0.0.59,SE=0.042	0.16
Effect of regularity in neg novelty responses in SST-cre recordings	S4f	Linear mixed effects model	102	F(1,202)=11.3808	β=0.21,SE=0.065	0.00089
Strength of optogenetic inactivation in VIP cells during tuning stimulus	S5a	Linear mixed effects model	36872	F(1,73742)=613.83	β=0.087,SE=0.0.0035	5.87e-135
Strength of optogenetic inactivation in PV cells during tuning stimulus	S5b	Linear mixed effects model	24744	F(1,49486)=6962.9	β=0.38,SE=0.0.0045	<1e-20
Strength of optogenetic inactivation in SST cells during tuning stimulus	S5c	Linear mixed effects model	6968	F(1,13934)=2236.0	β=0.41,SE=0.0.0087	<1e-20
Effect of light in normal sessions and control sessions	s6b,d	Linear mixed effects model	nAll =8573 nCtrl=284	F(1, 2978)All=794.420 F(1, 2978)Ctrl=3.240 F(1, 2978)Interaction=114.098	All = 0.455 Ctrl = 0.06 Interaction = -0.39	3.88e-155 0.072 3.67e-26
LME for effects of context and optogenetic inactivation of VIPs on negative deviance responses	s7e,f,g,h	Linear mixed effects model	1062	F(1, 4244)LIGHT=196.62 F(1, 4244)REGRND=0.83 F(1, 4244)Interaction=2.78	LIGHT= 0.20 REGRND=0.013 Interaction=-0.048	1.06e-43 0.36 0.095
LME contrasts for REG, RND, and base sound response, VIP optogenetic inactivation	s7f	Linear mixed effects model	1062	F(1,4244)RNDLIGHTNOLIGHT=76.31 F(1,4244)REGLIGHTNOLIGHT= 123.10 F(1,4244)LIGHTREGRND= 3.33 F(1,4244)NOLIGHTREGRND=0.29	RNDLNL = 0.18 REGLNL = 0.23 LIGHTRR = 0.037 NOLIGHTRR = -0.011	3.44e-18 3.24e-28 0.068 0.59
Baseline sound response, VIP inactivation	s7f	t-test	1062	MeanNOLIGHT=0.0703 MeanLIGHT=-0.0146	n/a	1.9e-07 0.27
Effect of inactivation of VIPs on baseline sound response	s7f	paired t-test	1062	MeanDifference=-0.213	n/a	2.67e-13

LME for effects of context and optogenetic inactivation of PVs on negative deviance responses	s7i,j,k,l	Linear mixed effects model	662	F(1, 2644)LIGHT=217.52 F(1, 2644)REGRND=1.88 F(1, 2644)Interaction=0.078	LIGHT= 0.299 REGRND=0.028 Interaction=0.011	2.27e-47 0.17 0.78
LME contrasts for REG, RND, and base sound response, PV optogenetic inactivation	s7j	Linear mixed effects model	662	F(1, 2644)RNDLIGHTNOLIGHT=112.92 F(1, 2644)REGLIGHTNOLIGHT= 104.68 F(1, 2644)LIGHTREGRND= 0.59 F(1, 2644)NOLIGHTREGRND=1.36	RNDLNL = 0.31 REGLNL = 0.29 LIGHTRR = 0.022 NOLIGHTRR = 0.033	7.42e-26 4.01e-24 0.44 0.244
Baseline sound response, PV inactivation	s7j	t-test	662	MeanNOLIGHT=0.0021 MeanLIGHT=0.25	n/a	0.87 7.42e-17
Effect of inactivation of PVs on baseline sound response	s7j	paired t-test	662	MeanDifference=-0.248	n/a	5.99e-17
LME for effects of context and optogenetic inactivation of SSTs on negative deviance responses	s7m,n,o,p	Linear mixed effects model	238	F(1, 948)LIGHT=74.88 F(1, 948)REGRND=24.14 F(1, 948)Interaction=0.67	LIGHT= 0.29 REGRND=-0.16 Interaction=0.055	2.12e-17 1.06e-06 0.41
LME contrasts for REG, RND, and base sound response, SST optogenetic inactivation	s7n	Linear mixed effects model	238	F(1, 948)RNDLIGHTNOLIGHT=44.85 F(1, 948)REGLIGHTNOLIGHT= 30.69 F(1, 948)LIGHTREGRND= 16.42 F(1, 948)NOLIGHTREGRND=8.38	RNDLNL = 0.32 REGLNL = 0.27 LIGHTRR = -0.19 NOLIGHTRR = -0.14	3.63e-11 3.92e-08 5.48e-05 0.0039
Baseline sound response, SST inactivation	s7n	t-test	238	MeanNOLIGHT=-0.0917 MeanLIGHT=0.205	n/a	8.60e-07 1.22e-05
Effect of inactivation of SSTs on baseline sound response	s7n	paired t-test	238	MeanDifference=-0.113	n/a	0.011